UNIVERSIDADE FEDERAL DO PARANÁ

CLARA INÉS GARCÍA MARTÍNEZ

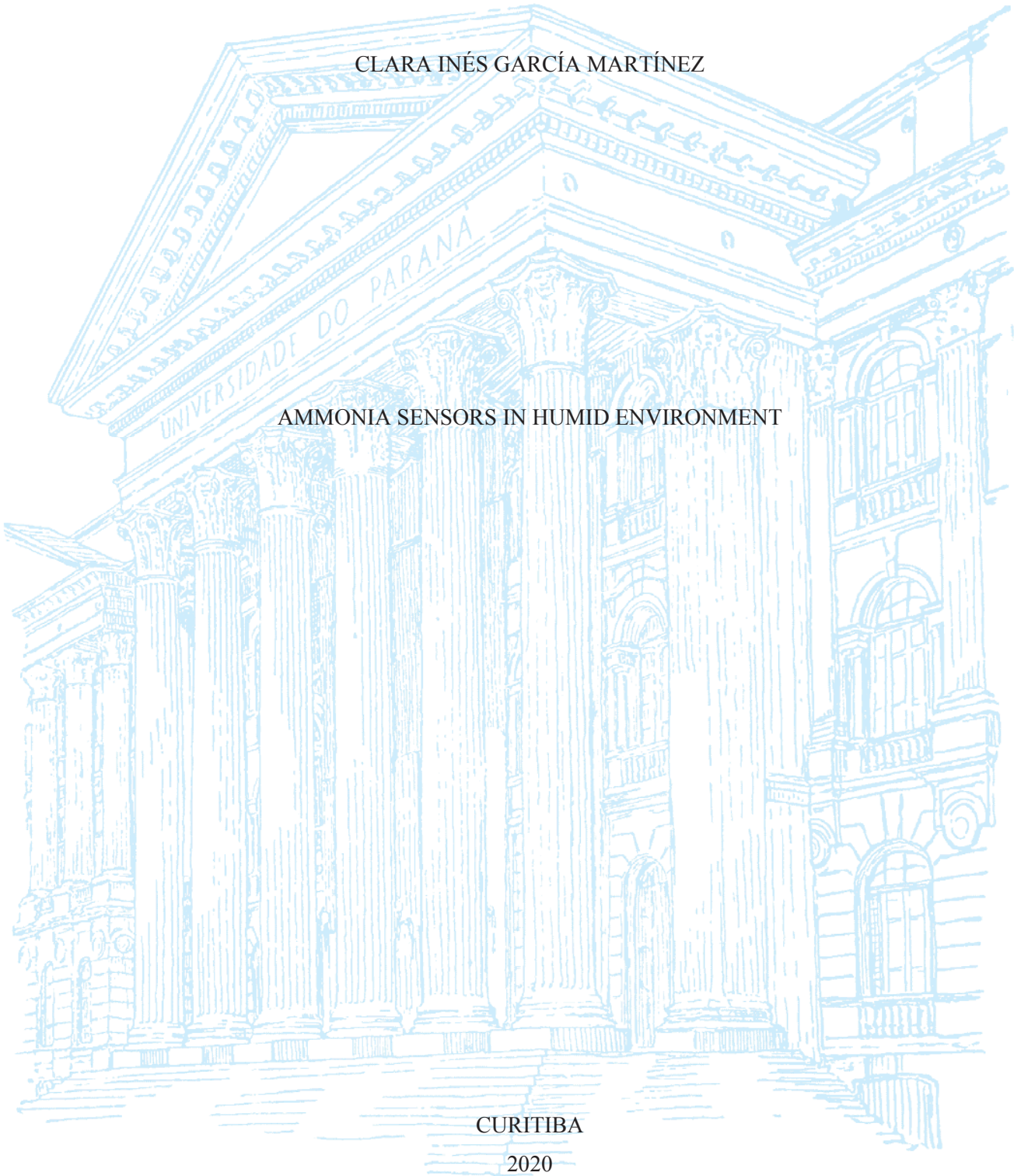


# AMMONIA SENSORS IN HUMID ENVIRONMENT

CURITIBA

2020

CLARA INÉS GARCÍA MARTÍNEZ

# AMMONIA SENSORS IN HUMID ENVIRONMENT

Dissertação apresentada ao curso de Pós-Graduação em Engenharia e Ciência dos Materiais, Setor de Tecnologia, Universidade Federal do Paraná, como requisito parcial à obtenção do título de Mestre em Engenharia e Ciência dos Materiais.

Orientador: Prof. Dr. José Pedro Mansueto Serbena/Ivo A. Hümmelgen

CURITIBA

2020

Catalogação na Fonte: Sistema de Bibliotecas, UFPR
Biblioteca de Ciência e Tecnologia

G111a García Martínez, Clara Inés
Ammonia sensors in humid environment [recurso eletrônico] / Clara Inés García Martínez. – Curitiba, 2019.

Dissertação - Universidade Federal do Paraná, Setor de Tecnologia, Programa de Pós-Graduação em Ciência e Engenharia de Materiais, 2019.

Orientador: José Pedro Mansueto Serbena – Coorientador: Ivo Alexandre Hümmelgen.

1. Amônia. 2. Deposição de vapor químico. 3. Materiais nanoestruturados. 4. Carbono. I. Universidade Federal do Paraná. II. Serbena, José Pedro Mansueto. III. Hümmelgen, Ivo Alexandre. IV. Título.

CDD: 546.7112

Bibliotecário: Elias Barbosa da Silva CRB-9/1894

MINISTÉRIO DA EDUCAÇÃO
SETOR DE CIENCIAS EXATAS
UNIVERSIDADE FEDERAL DO PARANÁ
PRÓ-REITORIA DE PESQUISA E PÓS-GRADUAÇÃO
PROGRAMA DE PÓS-GRADUAÇÃO ENGENHARIA E CIÊNCIA DOS MATERIAIS - 40001016033P9

# TERMO DE APROVAÇÃO

Os membros da Banca Examinadora designada pelo Colegiado do Programa de Pós-Graduação em ENGENHARIA E CIÊNCIA DOS MATERIAIS da Universidade Federal do Paraná foram convocados para realizar a arguição da dissertação de Mestrado de **CLARA INÉS GARCÍA MARTÍNEZ** intitulada: **Ammonia Sensors in Humid Environment**, sob orientação do Prof. Dr. JOSÉ PEDRO MANSUETO SERBENA, que após terem inquirido a aluna e realizada a avaliação do trabalho, são de parecer pela sua APROVAÇÃO no rito de defesa.

A outorga do título de mestre está sujeita à homologação pelo colegiado, ao atendimento de todas as indicações e correções solicitadas pela banca e ao pleno atendimento das demandas regimentais do Programa de Pós-Graduação.

CURITIBA, 21 de Fevereiro de 2020.

JOSÉ PEDRO MANSUETO SERBENA
Presidente da Banca Examinadora (UNIVERSIDADE FEDERAL DO PARANÁ)

VITOLDO SWINKA FILHO
Avaliador Interno (UNIVERSIDADE FEDERAL DO PARANÁ)

RICARDO CANUTE KAMIKAWACHI
Avaliador Externo (UNIVERSIDADE TECNOLÓGICA FEDERAL DO PARANÁ)

To the memory of my late advisor, Ivo Alexandre Hümmelgen.

## ACKNOWLEDGMENTS

I would thank all the people who have contributed with their help in the achievement of all my goals, during the research work carried out as reported herein. Many people have contributed to the development and completion of this work with their advice, assistance, encouragement, and generosity, which gave me strength along this study when I needed it the most. I tried and worked hard knowing that it was not going to be easy to travel alone in the academic journey without their support. I cannot express my total recognition deserved by every person in this text. However, solemnly I want to say, “all your efforts towards grooming me are highly appreciated.”

The deep sense of appreciation goes to my late father Mario García, who gave me one of the greatest advices since my childhood *"Clarita, study and know the world"*. After all, I thank God for my parents, my health and life as well as the opportunity he gave me to meet the late Professor Ivo Alexandre Hümmelgen, who transferred to me the idea of this project. Professor Ivo Alexandre Hümmelgen supported me personally and institutionally and gave me motivation for working hard.

Thanks to my FAMILY, teachers, advisors, friends, co-workers and colleagues for their wonderful support. To the members from my latest research group (Organic optoelectronic devices (GOOD)), the collaborators in Africa, the Latinos, my landlady, neighbors, all the people I met in this experience of being out of my country Colombia, and the list goes on. I express my sincere admiration to the Brazilian government for the opportunity of realize post-graduate studies through scholarships offered to foreigners like myself, as well as to Portaria N° 206 de 4 de setembro de 2018 da Coordenação de Aperfeiçoamento de Pessoal de Nível Superior (CAPES), for the financial support given through a scholarship program including the post-graduate program in Material Science and Engineering of the Universidade Federal do Paraná.

Finally, I thank the professor and advisor José Pedro Serbena, Dr. Rafael Rodriguez and Dr. Isidro Cruz Cruz who greatly helped me to conclude this work with their knowledge, technical skills and inspiration.

This work might help you understand the functioning and importance of the sensors in your day to day learning process.

*Jovem, a trabalhar...Divirta-se!* (Ivo A. Hümmelgen)

## RESUMO

Neste estudo, a melhoria do comportamento de detecção de vapor de amônia em ambiente úmido foi investigada. A investigação incluiu a fabricação e caracterização de diferentes sensores baseados em vários materiais nanostruturados: esferas ocas de carbono recozidas (HCSs), HCSs dopadas com nitrogênio (N-HCSs-10 e 50), nitreto de gálio (GaN), GaN revestido de carbono (C-GaN TA e TN) e nanotubos de carbono de paredes múltiplas dopadas com nitrogênio alinhados (A-CNTs). Isso foi feito para avaliar a capacidade de detectar e discriminar amônia e água. A resposta dos sensores foi investigada através de medições de resistência em função da concentração dos analitos e frequência de operação, em condições controladas (ou seja, temperatura: ~23 °C, umidade relativa: ~20% e atmosfera inerte (nitrogênio)). Os baixos limites de detecção de amônia (6 ppm) foram estabelecidos para os sensores baseados em N-HCSs. Foi descoberto que a dependência de água para as N-HCSs era menor que para das HCS não dopadas. Assim, os resultados sugeriram que as nanoestruturas N-HCSs são potenciais candidatos a dispositivos sensoriais ambientais insensíveis à umidade para a detecção de vários vapores químicos. O GaN, C-GaN TN e C-GaN TA apresentaram resposta positiva quando expostos a amônia e água. A maior sensibilidade foi alcançada para nanoestruturas C-GaN TN quando expostas a amônia, enquanto a menor sensibilidade foi determinada para as moléculas de água. Por outro lado, os dispositivos baseados em A-CNTs não apresentaram resposta à amônia e à água, e foram feitas algumas recomendações para possíveis trabalhos futuros com este material. Este trabalho também consiste na análise baseada em três sensores selecionados (por exemplo, C-GaN TN, HCSs e N-HCSs 50) expostos à mistura de amônia e água, aplicando-se à metodologia generalizada de tristímulos. As medições binárias da mistura foram realizadas em umidades relativas de 100%, 75%, 50%, 25% e 0%, constatando que as respostas as diferentes concentrações relativas de amônia e água são identificáveis.



Palavras-chave: Sensores de vapor químico. Materiais nanoestruturados. Esferas ocas de carbono. Amônia. Análise tristimulus.

## ABSTRACT

In this study, the improvement of the ammonia vapor sensing behavior in humid environment was investigated. The investigation included the fabrication and characterization of different sensors based on various nanostructured materials: annealed hollow carbon spheres (HCSs), nitrogen-doped HCSs (labeled as N-HCSs-10 and 50, depending on their particular synthesis conditions), gallium nitrate (GaN) and carbon-coated GaN nanoparticles (C-GaN-TA and TN) and finally aligned nitrogen doped multi-walled carbon nanotubes (A-CNTs). This was done in order to assess the ability to detect and discriminate ammonia and water. The sensors response was investigated through resistance measurements as a function of both analyte concentration and operating frequency under controlled conditions (temperature: ~23 °C, relative humidity, RH: ~20% and inert atmosphere (nitrogen)). The low limit of detection for ammonia (6 ppm) was established for the N-HCSs-based sensors. It was discovered that the water dependency for the N-HCSs was lower than that for the un-doped HCSs. Thus, the results suggest that the N-HCSs nanostructures are potential candidates for humidity-insensitive environmental sensing devices for the detection of several chemical vapors. Concerning to GaN, C-GaN TN and C-GaN TA nanoparticles, they showed good response when exposed to ammonia and water. The higher sensitivity for this kind of sensors was achieved for ammonia when C-GaN TN was used, whereas the lower sensitivity was obtained for water molecules. On the other hand, the devices based on A-CNTs (synthesized under several conditions) showed no response to ammonia and water, and some recommendations are made for possible future work with this material. This work also consists on the analysis based on three selected sensors (i.e. C-GaN TN, HCSs and N-HCSs 50) exposed to the mixture of ammonia and water, applying the generalized tristimulus methodology. The measurements of the binary mixture were performed at the relative humidities of 100%, 75%, 50%, 25% and 0%, finding that the responses to different relative concentrations of ammonia and water are identifiable.



Keywords: Chemical vapor sensors. Nanostructured materials. Hollow carbon spheres. Ammonia. Tristimulus analysis.

**TABLE OF CONTENTS**

**1 INTRODUCTION ..... 10**

1.1 MOTIVATION ..... 11

1.2 OBJECTIVES ..... 12

1.2.1 Overall Purpose ..... 12

1.2.2 Specific objectives ..... 12

1.3 METODOLOGY ..... 12

**2 LITERATURE REVIEW ..... 14**

2.1 DEFINITIONs ..... 14

2.2 SENSOR CLASSIFICATION ..... 15

2.2.1 Optical sensors ..... 15

2.2.2 Mass sensors ..... 16

2.2.3 Electrochemical sensors ..... 16

2.2.4 Resistivity sensors ..... 17

2.3 SENSING MATERIALS ..... 18

2.4 ADSORPTION PHENOMENON ..... 19

2.5 ELECTRICAL MEASUREMENT ..... 21

2.6 SENSOR PERFORMANCE EVALUATION ..... 23

2.6.1 Calibration curve ..... 23

2.6.2 Signal to noise ratio (SNR) ..... 24

2.6.3 Sensitivity ..... 24

2.6.4 Selectivity ..... 25

2.6.5 Detection and Quantification limits ..... 26

2.6.6 Time factors: Response time and Recovery time ..... 27

2.7 TRISTIMULUS ANALISYS ..... 28

**3 MATERIALS AND METHODS ..... 32**

3.1 MATERIALS ..... 32

3.1.1 Interdigitated electrodes ..... 32

3.1.2 Nanomaterials ..... 32

3.1.3 Chemicals ..... 36

3.2 METHODS ..... 36

3.2.1 Preparation of nanomaterial dispersions using a surfactant method ..... 36
3.2.2 Sensor fabrication and gas sensing measurements ..... 37

**4 RESULTS ..... 39**

4.1 CHARACTERIZATION OF MATERIALS ..... 39
4.1.1 Sensors based on annealed HCSs, N-HCSs-10 and N-HCSs-50 ..... 39
4.1.2 Sensors based on carbon coated GaN (C-GaN) ..... 44
4.1.3 Aligned nitrogen doped multi-walled carbon nanotubes (A-CNTs) ..... 50
4.1.4 Comparison of results with literature ..... 51
4.1.5 Material selection ..... 52
4.1.6 Response and recovery time ..... 54
4.2 TRISTIMULUS ANALISYS ..... 55

**5 CONCLUSIONS ..... 57**

5.1 FUTURE DIRECTIONS ..... 58

**REFERENCES ..... 59**

**APPENDIX 1–EVALUATION OF DIFERENT ANALYTES ..... 63**

**APPENDIX 2 – SCIENTIFIC CONTRIBUTIONS ..... 71**

**APPENDIX 3 – PARTICIPATION ON CONGRESS AND/OR COURSES ..... 72**

# 1 INTRODUCTION

Consider the following experience or situation: the aroma of a Colombian coffee cup stimulates the receptors in our nose every morning. From that moment, our brain begins to analyze the different organoleptic properties of this aromatic drink (odor, taste, color, temperature, among others). In this manner, the brain translates all of it into sensations and even memories. This phenomenon applies to any coffee, other foods or aromas, but Colombian coffee is famous for its characteristics. Perception is possible because of the existence of several sensors in our body, among them, the most important are tongue, nose, ears, eyes and skin. Similarly, in our actual society, we have developed electronic elements or devices that are capable of detecting external stimuli and, as a consequence, show a response.[1]

Sensor is defined as a measuring device that detects (senses) a phenomenon (such as heat, light, sound, pressure, magnetism, motion, composition, presence of a particular element or ion, concentration, chemical activity, partial pressure, etc.) and conveys or translates this information in a certain manner, usually of electrical nature.[2]

Ammonia gas ($NH_3$) sensors based on carbon materials lately received important attention due to their promising sensitivity towards this compound. The concern is to control toxic gases particularly in areas such as medical field, aerospace, integrated circuits, food industries, farming industries, environmental science, national security sector and many more.[3–6] This can further offer possible explorations of inexpensive materials that are capable of detecting ammonia at room temperature.[7–18]

Ammonia is one of the industrial chemicals most extensively used.[19] It is a chemical precursor widely utilized in the synthesis of fertilizers, explosives, detergents, pharmaceuticals among other compounds.[20] Particularly, in Colombia, 80% of the illegal explosive devices are fabricated with ammonia as precursor. Thus, ammonia detection is of paramount importance for national security.[21] In addition, despite its widespread use, ammonia is highly toxic and, under frequent exposure, it induces lung disease, liver failure and urea cycle disorder with the consequent brain damage.[20] In this manner, detection and quantification of ammonia is also crucial for environmental, industrial, and biomedical purposes.[22]

Most of the people can identify ammonia odor at a concentration of 35 $mg/m^3$ (or 49.7 ppm since 1 $mg/m^3$ is about 1.42 parts per million). Occupational atmospheric exposure is usually regulated to a limit of 18-40 $mg/m^3$ (or equivalently 25.56 – 56.8 ppm).[23] That is the reason why there is an impelling demand for a reversible, robust and accurate sensor able to monitoring ammonia.

There are many ways to detect a gas, such as chromatography, mass spectrometry technologies, as well as electrochemical, mass and optical sensors. Low cost devices, such as infrared sensors, may present some issues when the application demands accuracy. These problems are related with the low absorption profile of ammonia. Electrochemical detectors using polymeric films have advantages, such as the possibility to work at room temperature and the possibility to detect a large amount of gas.[24]

A particular kind of sensors are based on nanomaterials, with dimension of less than 100 nm (which implies that they show quantum effects) and surface-area-to-volume ratio greater than that in bulk materials. Therefore, due to their quantum nature they behave significantly different from bulk materials,[25] causing an enhancement in their chemical reactivity, as well as improvement in their mechanical, optical, electrical and magnetic characteristics.[26]

An important tool in the description (or characterization) of chemical sensors is the tristimulus methodology, which was developed in the Group of Organic and Optoelectronic Devices by I. A. Hümmelgen and co-authors.[27–29] Briefly, similar to determination of a particular color through chromaticity coordinates (RGB coordinates), the quantification of a single analyte with three different sensors in a mixture of components is possible.

## 1.1 MOTIVATION

Gas sensors have been acknowledged as simple and inexpensive tools for detection and quantification of toxic, harmful, flammable and explosive gases. It is well known that gas sensors are devices composed of active sensing materials coupled to a signal transducer. Because of these materials directly interact with the analyte, their selection, study and development play an important role in the design of high performance gas sensors.[30]

The measurements of ammonia gas in real time and under several conditions have limits for their applicability, such as, high cost and low practicality. For example, the price for conventional analytical instruments like gas chromatography-mass spectrometry (GC-MS)[31] amounts to $50,000 USD,[32] whereas special sensors operating at high pressures/temperatures, require an equipment sizing of 0.16 $m^3$.[33] Particularly, environmental factors such as temperature and moisture affect the performance of chemical sensors. Thus, the study of the ammonia sensors under these conditions is relevant for their applicability in a humid environment.[34,35]

Concerning the study on ammonia detection involving humid environments, Mutuma et al[36] reported the ammonia vapor sensing behavior of hollow carbon spheres (HCSs), a hollow carbon sphere–polyvinylpyrrolidone (HCS/PVP) composite and annealed hollow carbon spheres. In that study, they showed the best ammonia response of the annealed HCS materials was at 33% relative humidity. Importantly, the ammonia response and sensitivity of the annealed HCSs were found to be higher than those reported in the literature. Similar studies were reported, for example, by Sangaletti and co-workers,[37] which studied single-walled carbon nanotubes (CNT's) under real conditions of room temperature and humidity.

## 1.2 OBJECTIVES

### 1.2.1 Overall Purpose

Optimize the complete set of parameters that determine the best performance on ammonia gas sensors operating under both different relative humidities and analyte concentrations. Among possible parameters, several kinds of nanoparticles, operating parameters, ammonia concentrations and relative humidities will be considered.

### 1.2.2 Specific objectives

- ✓ Determine the active material based on nanoparticles with the best sensing response to ammonia and water.
- ✓ Design an experimental set-up for the complete control of the variables under study like electrical parameters, relative humidity and ammonia concentration.
- ✓ Apply the tristimulus (or n-stimuli) methodology for device characterization.

## 1.3 METODOLOGY

This research was developed as follows:

1. Literature review. State-of-the-art on sensors based on nanostructures in order to identify possible research opportunities and issues to be solved.
2. Learning of adequate experimental techniques applied to sensor devices.

3. Evaluation of sensors based on different types of nanoparticles when they are exposed to a set of analytes, in order to select the materials with the best sensing properties to detect ammonia and water.
4. After selection of the appropriate sensing materials, the best operating conditions will be identified. It is expected the optimization of the sensitivity, the detection and quantification limits, as well as response and recovery times.
5. Finally, the set of sensors will be evaluated simultaneously in an ammonia environment at several relative humidities, after that, the results will be analyzed using tristimulus methodology.

# 2 LITERATURE REVIEW

A literature review on definitions and components of a sensor, classification of sensors, detection phenomena, sensing materials, measurements, sensor characterization and analysis tools is presented.

## 2.1 DEFINITIONS

Following the R. W. Catterall's book[38] definition, a chemical sensor is "*a device which responds to a particular analyte in a selective way through a chemical reaction and can be used for the qualitative or quantitative determination of the analyte. Such a sensor is concerned with detecting and measuring a specific chemical substance or set of chemicals.*"

Chemical sensors translate chemical information (composition, concentration, chemical activity, partial pressure, etc.) into an analytically measurable signal (optical, electrical, etc.). The desirable advantages of chemical sensors are: short analysis time, reduced size, ease of operation, very low power consumption, the possibility of acquiring the measurement and obtaining the result in place, deliver information in real time and on-line on the presence of specific compounds or ions in even complex samples.[39,40]

Chemical sensors generally contain two basic components connected in series: a chemical (molecular) recognition (receptor) system and a physico-chemical transducer (Fig.1).

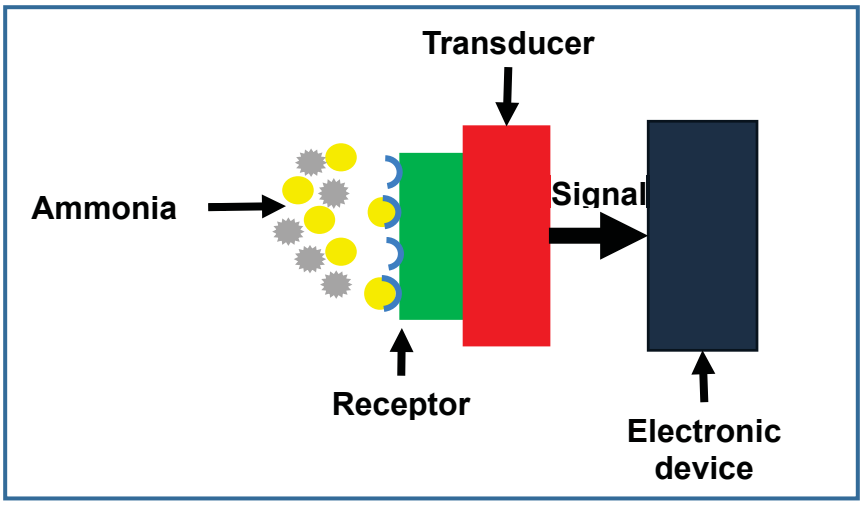


Figure 1 – Scheme of basic components of a chemical sensor. Adapted of A. Bandodkar and J. Wang (2014).[41]

In most chemical sensors, the receptor interacts with the analyte molecules. As a result, their physical or chemical properties are altered in such a way that the attached transducer can gain an electrical signal. In gas sensor based on carbon nanostructures, for example, the same element acts as receptor and as transducer due to their electrical conductivity change in contact with some gases or analytes.[42] The interaction of the analytes alter the electronic cloud of the semiconductors, thereby changing the energy levels accessible to the load carriers, that is, the electronic transport.

In many cases, the receptor is a thin layer that is able to interact with analyte molecules. The receptor enables the sensor to respond selectively to a particular substance or group of substances. Adsorption is the most important process in chemical sensors, among others. This phenomenon acts at the interface between the surface of the analyte and the receptor, where both are in an equilibrium state.[2]

The transducer is where the signals are processed, almost exclusively by means of electrical instrumentation. The actual concentration value, a non-electric quantity, must be transformed into an electrical one: voltage, current or resistance.[42]

## 2.2 SENSOR CLASSIFICATION

There are different criteria for classifying chemical sensors,[43] according to operating principle, analyte (sensors for H+, for metal ions or for determining oxygen or other gases), field of application (for example sensors intended for use in vivo, or sensors for monitoring process), etc.[40]

Based on the work by Adam Hulanicki, et al,[44] the chemical sensors are classified according to the operating principle of the transducer in four groups: optics, mass sensitive, electrochemical and electrical conductivity (or resistivity) sensors.

### 2.2.1 Optical sensors

Optical sensors are based on detection of a beam of light or other electromagnetic waves during the interaction with the chemical species which are desired to determine. The physical principles and arrangements developed in the area of optical sensors for detection of gases are numerous. Therefore, there are different methods of signal detection, for example: infrared detectors (work with signals in the infrared spectrum) and photoionization (signals located in the ultraviolet region of the spectrum).[45]

### 2.2.2 Mass sensors

These types of sensors are based on microgravimetry, that is, the measurement of mass changes that occur as a characteristic of the interaction of chemical species with the sensor. Its design consists of a piezoelectric material subjected to oscillation. The response of these devices depends on the changes in their resonant frequency, or base frequency, which is a function of the mass variations of the chemical species deposited as a coating on the sensor, during the detection. The resonance frequency depends mainly on the thickness of the piezoelectric crystal, the coating of the sensing phase and the visco-elastic properties of the crystal.[45] Fig. 2 shows an example of a mass sensors used during thermal deposition of materials under vacuum conditions.

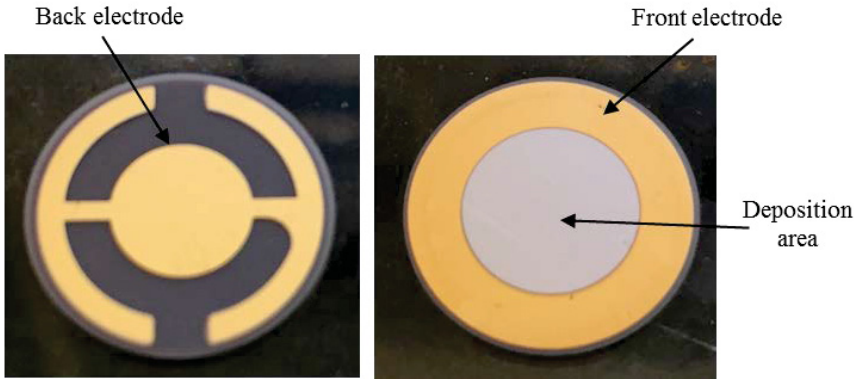


Figure 2 – Gold coated piezoelectric crystals (in this case, an INFICON ™ sensor).

### 2.2.3 Electrochemical sensors

This is an important and largest class of chemical sensors, being used to detect the most diverse molecules, microorganisms, among others. The inherent principle is that one or more chemical reactions eventually produce or use ions and/or electrons that cause changes in the electrical properties of samples.[46]

The basic components of an electrochemical sensor are a working electrode (or sensor), a reference electrode and a counter electrode. These electrodes are placed in the sensor box in contact with a liquid electrolyte. The working electrode is on the inner face of a membrane which is porous to the analyte but impermeable to the electrolyte, resulting in an electrical voltage between the terminals (Fig.3).

Electrochemical sensors are classified as potentiometric, voltammetric and conductimetric. The mechanism of operation depends mainly on the physical principle that governs them according to their classification, presenting some similarities regarding the measured signal.[45] A comparison among the operating principles in sensors is shown in the Table 1.

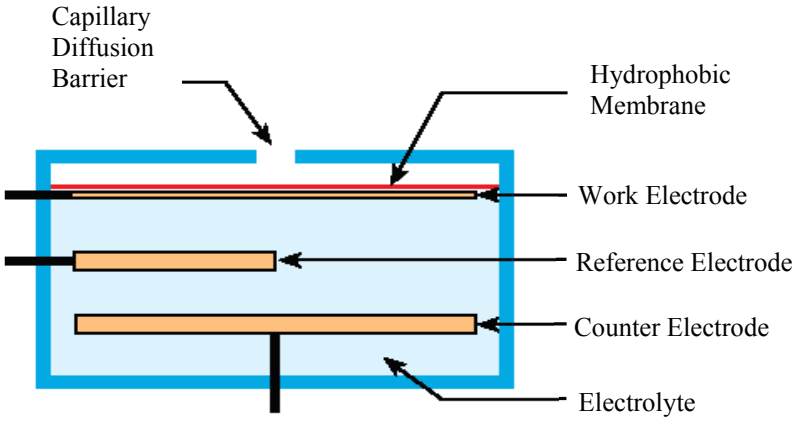


Figure 3 – Typical electrochemical sensor setup.[47]

Table 1 – Transducer principles and measuring techniques of electrochemical sensors.[42]

| Sensor | Transducer principle | Measured quantity |
|---|---|---|
| **Potentiometric** | Energy conversion | Voltage (high impedance) |
| **Amperometric** | Limiting current | Current (low impedance) |
| **Conductimetric or impedimetric** | Resistive | Resistance (reciprocal of conductance) |

### 2.2.4 Resistivity sensors

Resistivity sensors based on organic semiconductors (carbon nanoparticles) are used in this study, however, the following operating mechanism of this type of sensors also applies to inorganic materials, such as metal oxides, where the signal comes from the change in the electrical properties caused by the interaction of the analyte with the receptor layer.[42] This is due to the sensitivity that some materials possess when exposed to gases and vapors, which react producing a change in their electrical resistance. Materials typically used by its low cost and ease of resistance measurement are organic semiconductors.[48]

As a case of study about this kind of sensors, the system conducting polymer-gas molecules possibly undergo different mechanisms of interaction, not necessarily following the

same sequence, such as those shown in Fig. 4. In the interaction process, charges are firstly transferred between the polymer and the electrode contact as an effect of the analyte molecule X (process 1 in the fig. 4). This is followed by the second process (process 2) whereby either oxidation or reduction of the polymer chain caused by the analyte, resulting in the density of charge carriers being changed during the process. This happens rapidly to reactive gases such as ammonia and/or hydrogen sulfide. Thirdly, the backbone of the polymer exhibits mobile charge carriers, which allows the analyte to interact actively resulting in the carrier mobility along the polymer chain to be changed (process 3). Moreover, the charge carrier mobility along the polymer chain can be modulated such that the analyte easily interacts with the counterion ($C^-$) (process 4). Lastly, it is possible for the analyte to alter the probability of charge carriers that are moving around the polymer chains causing film resistivity (process 5). However, the first two processes together with the last one, can be encountered in organic semiconducting materials.[49]

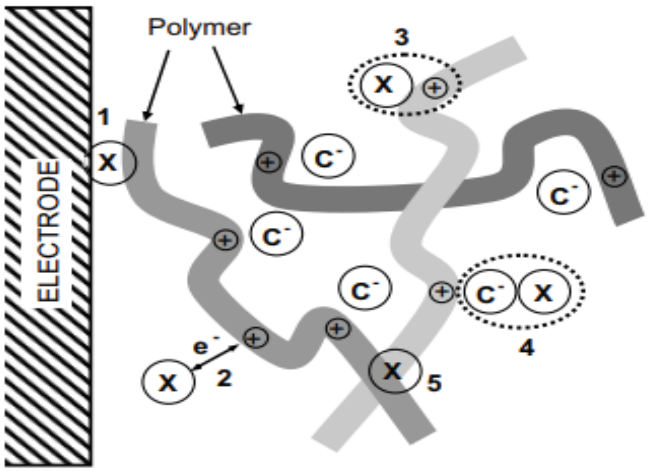


Figure 4 – Possible interaction of a gas molecule with a conducting polymer. X is the analyte; $C^-$ is the counterion.[49]

## 2.3 SENSING MATERIALS

Previous researches have shown the use of carbon structures in the active layer of an array of sensors to detect one or more compounds. The array is prepared with different carbon materials with a particular sensitivity to each component in a mixture[36,50–52] and the responses of the sensors to each analyte using mathematical models were analized.[36,52,53]

Gas detection using carbon-based materials such as graphene and carbon nanotubes, has been previously studied by different researchers.[16,54–58] The advantages of this type of

materials are their simple fabrication, large surface areas, low electrical noise, high conductivity, and outstanding electronic properties.[59]

Prior researches conducted at room temperature (*RT*) by Ghost R. et al[35] were based on graphene oxide and Yavari F. et al[60] using a macroscopic three-dimensional graphene foam network, reported limit of detection (*LoD*) for ammonia of 200 ppm and 20 ppm respectively, but they did not show the sensitivity value. Zhou Y. and co-workers[61] found a lower *LoD* for ammonia at *RT* of 2 ppm and sensitivity of $1.43 \times 10^{-2}$ $ppm^{-1}$ using ternary reduced graphene oxide-titanium dioxide-Au composite.

Ammonia sensors in humid environment (10–97%) at 40 °C based on Hollow Carbon Spheres (HCSs) and hollow carbon sphere/polyvinylpyrrolidone (HCS/PVP) composite were performed by Mutuma et al,[36] and the $NH_3$ sensitivity values (% per ppm) of the pristine HCSs, HCS/PVP and annealed HCSs were reported as 0.08, 4.0 and 1.6, respectively. The Table 2 shows that the resistance values measured in Mutuma's work (by annealed HCSs at 40 °C) were higher than those reported for other nanomaterial-based sensors at room temperature.

TABLE 2 – Comparison of ammonia sensors based on different materials.

| Materials | Relative resistance variation ($\Delta R/R_0$) | Minimum $NH_3$ concentration (ppm) |
|---|---|---|
| **RGO**[62] | 0.052 | 50 |
| **RGO-PANI**[62] | 0.592 | 50 |
| **Ag NC-MWCNTs**[63] | 0.09 | 10000 |
| **Activated carbon**[16] | 0.057 | 100 |
| **Oxidized activated carbon**[16] | 0.142 | 100 |
| **Pristine HCSs**[36] | 0.052 | 74 |
| **HCS/PVP**[36] | 0.46 | 74 |
| **Annealed HCSs**[36] | 0.66 | 74 |

## 2.4 ADSORPTION PHENOMENON

Microscopically all solids have a specific molecular configuration, which is in its lowest energy state when they are in thermodynamic equilibrium. Under ideal conditions, the solid is periodic and infinite, but in a real behavior, the shape and surface must be considered.

Near the surface, the interaction of the body with the environment must be considered since submerging the solid into a liquid or gas creates an interface between the solid and the surrounding medium to which it is exposed.

Depending on the nature and type of environment to which the solid is exposed, surface reactions may be solid-solid, liquid-solid and gas-solid. Non-ideal behavior occurs due to small imbalances in the charge distribution of molecules that result in a permanent or induced electrical dipole moment.

When there are solid gas interactions, in which the gas is known as adsorbate and the solid as adsorbent, bonds are formed between the two components. When the phenomenon is reversible it is known as adsorption-desorption; if it is irreversible, there is a possibility that a new compound is formed.[64,65]

The adsorption process can be physical or chemical; the first one (physisorption) happens due to weak interactions such as Van der Waals forces, the second occurs when ionic, covalent or hydrogen bonds takes place and reactions such as oxidation may also take place when the solid comes into contact with oxygen.

In chemical adsorption, or chemisorption, a greater amount of energy is required in comparison with the physical adsorption to achieve equilibrium or the minimum energy state of the system. In addition to chemical adsorption, activation energy is required for chemical reactions to be carried out. In an adsorption process, the adsorbed gas molecules reach a dynamic equilibrium with the free molecules of the system that were not adsorbed by the solid and for a finite time reach their state of minimum energy.[66] The energy as a function of distance in physisorption and chemisorption are schematically shown in Fig. 5.

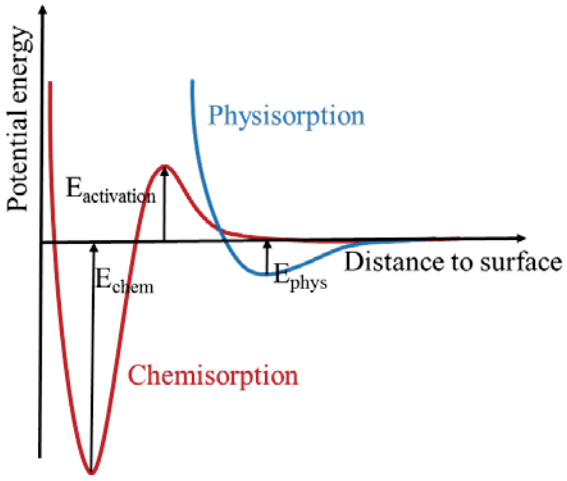


Figure 5 – Schematic potential energy diagram illustrating the difference between physisorbed and chemisorbed species.[67]

In order to study the solid-gas equilibrium, adsorption isotherms are usually carried out, which give the amount of gas adsorbed inside the solid at a certain external pressure, whereas the temperature remains constant throughout the entire process.[68]

Different thermodynamic models can be used to calculate the adsorption isotherms, among them, one is known as the Langmuir model.[69] In this model there are three basic postulates to describe adsorption on the surface of the solid:

1. Formation of a monolayer of adsorbed molecules.
2. All surface sites have the same probability of being occupied.
3. There is no interaction between adsorbed molecules.

The properties of the interface are recognized in the first and second postulates, the third postulate indicates that the changes in the surface properties associated with the adsorption of each molecule are constant, since there are no interactions between adsorbed species.[70]

## 2.5 ELECTRICAL MEASUREMENT

Sensor characterization is performed by measuring the electrical impedance (*Z*), with a LCR meter.[1] Impedance is a measure of the opposition to the flow of electric current. Impedance is not limited to Ohm's law for any current and voltage range and might depend of the frequency. Impedance is a *complex* quantity (in mathematical terms) composed of a *real* and an *imaginary* components.[42] Mathematically:

$$Z = Z' + iZ'' \tag{2.1}$$

For series circuits, the resistance is the real component of the impedance:

$$Z = R + i\,X \tag{2.1}$$

With magnitude defined as:

$$Z_0 = \sqrt{R^2 + X^2} \tag{2.2}$$

[1]Electronic test equipment used to measure the inductance (*L*), capacitance (*C*), and resistance (*R*) of an electronic component.

Where,

$Z'$ = Real part of impedance
$Z''$ = Imaginary part of the impedance
i = √-1
$Z_0$ = Magnitude of electrical impedance [Ω]
$R$ = Electrical resistance [Ω]
$X$ = Electrical reactance [Ω]

In a typical impedance measurement, a small signal is applied to a system, either voltage or sinusoidal current, with an specific amplitude and frequency, while monitoring the response in amplitude and phase. Finally, the current and the voltage are not precisely in phase. The perturbation signal as a function of frequency is expressed as a complex function as:[71]

$$V(\omega) = V_0 e^{i\omega t} \tag{2.3}$$

Where $V_0$ is the amplitude of the signal and $\omega$ is the frequency in radians/second, with $\omega = 2\pi f$ and $f$ expressed in Hertz. In a linear system, the response signal $I(t)$ can be expressed as:

$$I(\omega) = I_0 e^{i(\omega t - \emptyset)} \tag{2.4}$$

Where $I_0$ and $\emptyset$ are the amplitude and phase of the signal, respectively. Then, the impedance can be expressed as:

$$Z(\omega) = \frac{V(\omega)}{I(\omega)} = Z_0 e^{i\emptyset} = Z_0(cos\ \emptyset + isen\ \emptyset) \tag{2.5}$$

By this way, the real and imaginary components of the impedance are, respectively:

$$R = Z_0 cos\ \emptyset \tag{2.6}$$

$$X = Z_0 sen\ \emptyset \tag{2.7}$$

## 2.6 SENSOR PERFORMANCE EVALUATION

When measuring a sensor, only the relationships between its input stimulus and output signal are quantified and for this reason, it is important to apply analytical techniques to easily parameterize the operation of the system. In this section, the dynamic parameters used to characterize the performance of the sensors of this work are shown.[39,42]

### 2.6.1 Calibration curve

The calibration curve is a plot that shows how the response (electrical measurement in this study) changes as a function of the concentration of the analyte (the substance to be measured). The curve is adjusted by capturing the trend in the data by assigning a single function derived from some mathematical model. Sensor calibration function is described generically by a straight line, (such as in Fig. 6) expressed by the relationship.[72]

$$R_{es} = S[x] + b \tag{2.8}$$

With,

$R_{es}$ = Electrical response of the sensor
$[x]$ = Analyte concentration
$S$ = Sensitivity as a function of the analyte concentration $[x]$
b = Intercept on the y-axis, which gives the output signal for a zero input

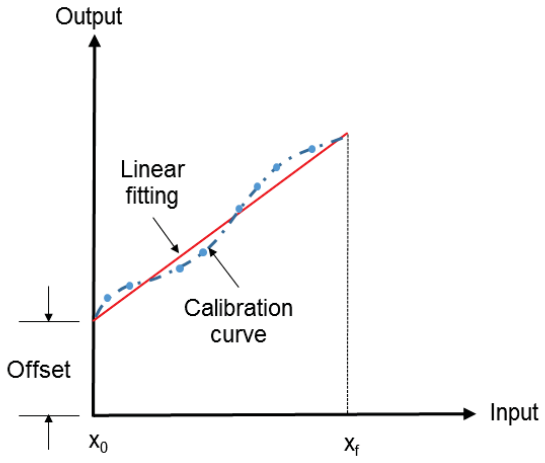


Figure 6 – Calibration curve example (with offset). Based on J. Webster (1999).[72]

### 2.6.2 Signal to noise ratio (*SNR*)

The *SNR* is defined as the average over time of the blank signal divided by the noise of the blank signal over the same time (Fig. 7). The following mathematical formula is used in statistics for calculating the signal to noise (*S/N*) ratio, in order to determine the quality of signal.[73]

$$SNR = \frac{Signal}{Noise} = \frac{\mu}{\sigma} \tag{2.9}$$

Where,

$\mu$ = Signal mean or expected value

$\sigma$ = Standard deviation calculation of the noise

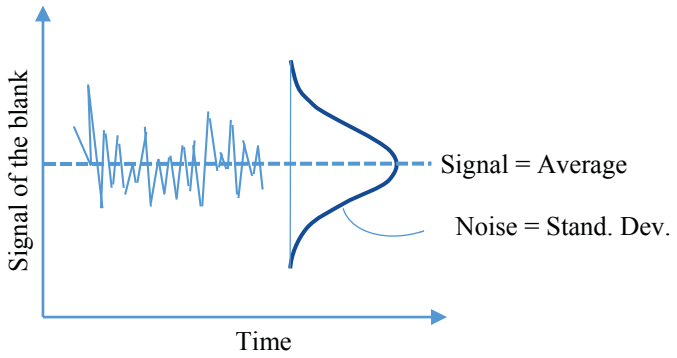


Figure 7 – Definition of *SNR*.

### 2.6.3 Sensitivity

Sensitivity is defined as change in the sensor response per concentration unit of the analyte, i.e. the slope of a calibration graph.[42] Therefore, the sensitivity goes from zero in the interference region, through a maximum in the dynamic range, to zero in the saturation region (Fig. 8). The sensitivity (*S*) of a sensor is the first derivative of its response (in this study the response $R_{es}$ is the relative resistance variation $R_{es} = \Delta R/R_0$), with respect to the concentration of the analyte, at any concentration [*x*] on the response curve. According to the Fig. 8, sensitivity is defined as:[74]

$$S = \frac{\partial\left(\frac{\Delta R}{R_0}\right)}{\partial[x]} \tag{2.10}$$

Where,

$\Delta R = R_f - R_0$

$R_f$ = The resistance of the sensor when exposed to analyte

$R_0$ = The resistance of the sensor in inert atmosphere ($N_2$) or background gas

$[x]$ = Analyte concentration

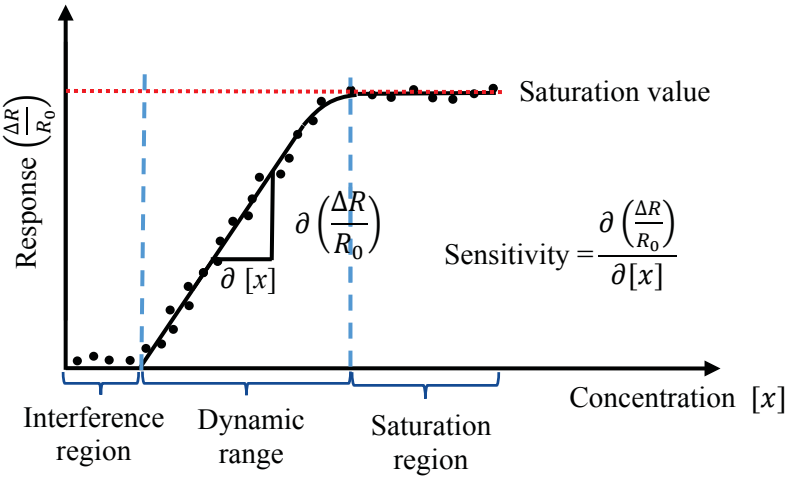


Figure 8 – Response curve. Based on J. Webster (1999).[72]

The sensitivity of the sensor has two sources of error: the standard deviation of the response ($\sigma R_{es}$) and the standard deviation of the concentration ($\sigma[x]$). If the calibration curve is nonlinear, the sensitivity will not be constant but will depend on the concentration of the analyte.

### 2.6.4 Selectivity

Janata J.[74] defined the selectivity as "*the ability of a sensor to respond primarily to only one species (analyte) in the presence of other species"*. Selectivity is an issue in chemical sensing, because one rarely knows the nature of the substance *a priori,* in addition to the similarity in the chemical nature of some substances into the system to be analyzed, such as detection of pollutants in the environment, disease detection, and other applications mentioned previously.[48] In order to find a solution to this problem of selectivity, an arrangement of sensors and analysis tools will be used in this study.

The quantitative expression used to sensor selectively response is adapted from Göpel W. et al:[75]

$$Z_a = \frac{\left(\frac{\Delta R}{R_0}\right)_a}{\sum_{k=1}^{n}\left(\frac{\Delta R}{R_0}\right)_k} \quad (2.11)$$

$Z_a$= Specificity for an analyte *a*

$\left(\frac{\Delta R}{R_0}\right)_a$ = Relative response for an analyte *a*

$\sum_{k=1}^{n}(\Delta R/R_0)$ = Sum of relative sensor response for analytes *k =1* to *n*

If $Z_a$ = 1, the sensor is selective only to the analyte *a.*

### 2.6.5 Detection and Quantification limits

Limit of Detection (*LoD*) is the lowest amount of analyte in the sample, which can be detected and that is significantly different from the blank, but not necessarily quantitated under stated experimental conditions.[76]

Limit of Quantification (*LoQ*) is the lowest amount of analyte in a sample, which can be quantitatively determined with suitable precision and accuracy.[76]

The approach used to calculate *LoD* is standard deviation of the blank. The blank determination is applied when the blank analysis gives results with a nonzero standard deviation.

Mathematically, and according with Fig 9, *LoD* and *LoQ* are defined as:[77]

$$LoD = X_b + 3\sigma_b \quad \text{and} \quad LoQ = X_b + 10\sigma_b \quad (2.12)$$

Where,

$X_b$ = mean response of the blank

$\sigma_b$= standard deviation of the blank

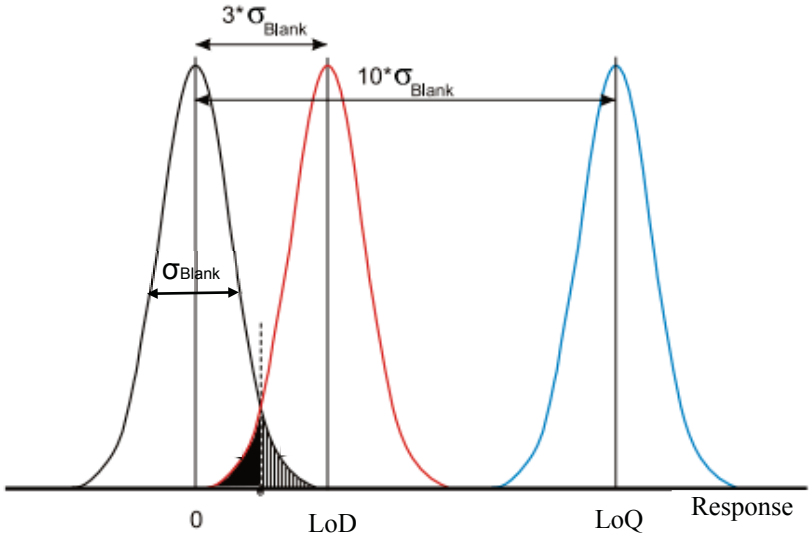


Figure 9 – *LoD* and *LoQ* response based on standard deviation of the blank.[78]

### 2.6.6 Time factors: Response time and Recovery time

The speed at which the sensor will detect the analyte (ammonia for example) and will be ready to measure again is an important characteristic of the sensor's performance. The calculations of time-related parameters are schematically illustrated in the Fig. 10.

This type of measurement indirectly shows the adsorption dynamics of the molecules by the active material, from the non-interaction state up to the dynamic equilibrium. This last state is called saturation, and the signal intensity can be related to interaction among different dipole moments and the active material, properties or structure of the active layer and finally, to the type of predominant interaction during the adsorption process (physisorption or chemisorption).[52]

Analyzing the response and recovery times it is possible to discern the type of interaction between the active layer and the analyte: if the interaction is weak, the signal returns to the initial response value, but if it is strong, the signal does not return to the initial value. In this last case, further treatments are necessary.

Response time is the interval time that takes to the sensor from its initial state (at zero concentration) up to a 90% of its response at its stabilized value (chemical equilibrium) when is exposed to the analyte concentration. Likewise, the recovery time is the required time for a 90% reversal of response variation to occur.[42,79]

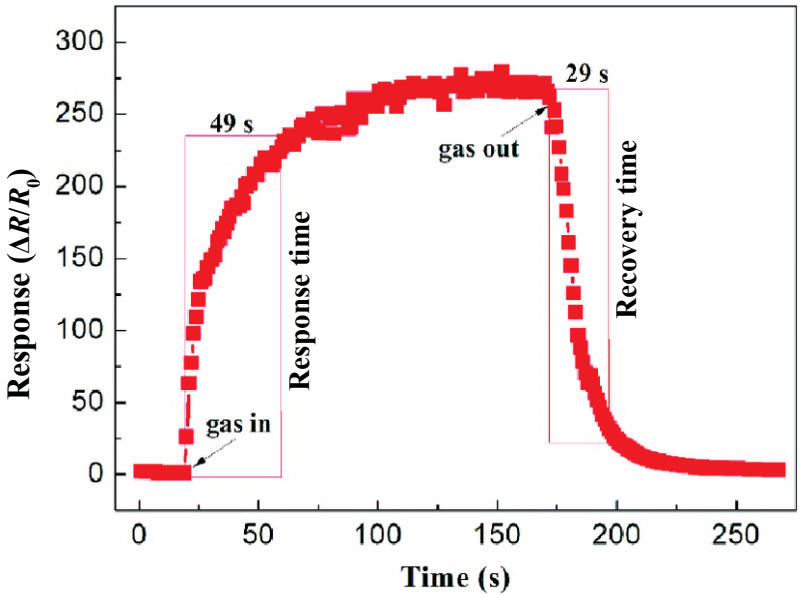


Figure10 – Example of the dynamic sensing, response-recovery time.[80] Response and recovery times are 49 s and 29 s, respectively.

## 2.7 TRISTIMULUS ANALISYS

Due to the difficulty in detecting only one analyte using a single sensor in a multiple analytes's environment, a set of multiple sensors have been used to achieve the detection of the specific analyte, as is the case with chemical sensors array using noses or electronic tongues. To determine the concentration of a substance in a mixture, tristimulus analysis can be used in which a set of three sensors is utilized during the analysis. This method of analysis was inspired by the concept of the human eye color reception. The concept involves a visual receptor system (i.e. the sense of sight) in which the cells existing in the retina of the eye, called cones, are specialized in detecting wavelengths coming from the environment and transforming them into electrical impulses. Thus the electrical impulses are then transported by the optic nerves to the brain, responsible for analyzing the information and producing the sensation of color.[29]

The perception of color in the brain can be explained by the additive mixing of certain amounts of red, green and blue light (RGB), in order to perceive other colors. For example, if the three light sources are mixed at maximum intensity, the human eye will perceive the color white. The mixture of the same three primary colors with less intensity will be perceived as a neutral gray. If the three sources are turned off, black is perceived.[81]

To numerically specify the color of a certain visual stimulus, colorimetry is based on the individual spectral sensitivities of the three types of conical cells, which constitute three stimuli values, created in this manner the tristimulus space. This same strategy was developed

by the research group of Professor Ivo. A. Hümmelgem[27,29,36] in order to apply it to a three sensors system, to know the concentration of a certain analyte in a mixture and assumed a linear response respect to analyte concentration.

The responses $I_i$ for three different sensors exposed to an analyte can be written as:

$$I_1 = \alpha[A],\ I_2 = \beta[A]\ \ and\ \ I_3 = \gamma[A] \tag{2.13}$$

Where,

$\alpha$, $\beta$ and $\gamma$ = sensitivities for every sensor.
$[A]$ = ammonia concentration.

For a binary mixture, the responses $I_i$, of the three sensors must consider the sensitivities to both analytes:

$$I_1 = \alpha_A[A]_r + \alpha_B[B]_r,\ I_2 = \beta_A[A]_r + \beta_B[B]_r\ \ and\ \ I_3 = \gamma_A[A]_r + \gamma_B[B]_r \tag{2.14}$$

$$[A]_r + [B]_r = 1 \tag{2.15}$$

Where,

$\alpha_A$, $\beta_A$ and $\gamma_A$ = sensitivities to the analyte A
$\alpha_B$, $\beta_B$ and $\gamma_B$ = sensitivities to the analyte B
$[A]_r$ = relative ammonia concentration.
$[B]_r$ = relative water concentration.

The response of each of the three sensors exposed to the analyte is taken as three components of a tristimulus vector (vector response), according with:

$$\vec{r} = \alpha[A]\hat{x} + \beta[A]\hat{y} + \gamma[A]\hat{z} \tag{2.16}$$

For a binary mixture, the vector responses, $\vec{r}$, of the three sensors must consider the sensitivities to both analytes:

$$\vec{r} = (\alpha_A[A]_r + \alpha_B[B]_r)\hat{x} + (\beta_A[A]_r + \beta_B[B]_r)\hat{y} + (\gamma_A[A]_r + \gamma_B[B]_r)\hat{z} \quad (2.17)$$

R. Rodriguez[29] developed a strategy to analyze sensors with negative or positive sensitivities to determine the relative concentration of an analyte in a binary mixture, called *the generalized tristimulus*. This strategy uses the coordinates of the point in which the tristimulus vector crosses a spherical shell with unitary radius, such as is represented in the Fig. 11, and according to the equation 2.18.

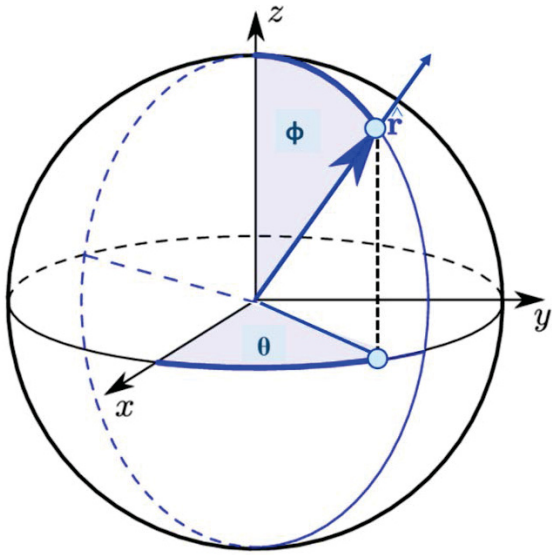


Figure 11 – Geometrical representation of the tristimulus vector crossing spherical shell with unitary radius showing the angles ϕ and θ that characterize the direction of the vector and the projection of the intersection point on the xy plane. Based on B. Mutuma (2017).[36]

$$\sqrt{{i_1}^2 + {i_2}^2 + {i_3}^2} = 1 \quad (2.18)$$

The coordinates of the point where the tristimulus vector crosses the spherical shell for one analyte, are given by the formulae below:

$$i_1 = \frac{I_1}{\sqrt{{I_1}^2+{I_2}^2+{I_3}^2}} = \frac{\alpha}{\sqrt{\alpha^2+\beta^2+\gamma^2}}, \quad i_2 = \frac{I_2}{\sqrt{{I_1}^2+{I_2}^2+{I_3}^2}} = \frac{\beta}{\sqrt{\alpha^2+\beta^2+\gamma^2}} \text{ and} \quad (2.19)$$

$$i_3 = \frac{I_3}{\sqrt{{I_1}^2+{I_2}^2+{I_3}^2}} = \frac{\gamma}{\sqrt{\alpha^2+\beta^2+\gamma^2}}$$

For a binary mixture, the coordinates of the point where the tristimulus vector crosses the unitary shell are given by the equations 2.20, obtained from equations 2.14 and 2.19:

$$i_1 = \frac{\alpha_B+(\alpha_A-\alpha_B)[A]_r}{ב} \quad i_2 = \frac{\beta_B+(\beta_A-\beta_B)[A]_r}{ב} \; i_3 = \frac{\gamma_B+(\gamma_A-\gamma_B)[A]_r}{ב} \tag{2.20}$$

Where,

$$ב = \sqrt{(\alpha_B + (\alpha_A - \alpha_B)[A]_r)^2 + (\beta_B + (\beta_A - \beta_B)[A]_r)^2 + (\gamma_B + (\gamma_A-\gamma_B)[A]_r)^2}$$

The relative concentration of the analyte is obtained from the equation 2.20. Knowing it is useful in practical applications.

$$[A]_r = \frac{\beta_B i_1-\alpha_B i_2}{i_2(\alpha_A-\alpha_B)+i_1(\beta_B-\beta_A)} \tag{2.21}$$

To represent positive and negative values of sensitivity is convenient to use angular coordinates. There are two angular coordinates (i.e. $\phi$ and $\theta$) that build-up a signature of the analyte of interest, with the coordinates confinement within the $0 \leq \phi < \pi$ and $-\pi \leq \theta < \pi$ intervals. Furthermore, equation 2.22 and 2.23 can be used to describe the point at which the vector crosses the unitary shell based on the two angular coordinates:

$$\phi = cos^{-1} \frac{I_3}{\sqrt{{I_1}^2+{I_2}^2+{I_3}^2}} \tag{2.22}$$

$$\theta = tan^{-1} \frac{I_2}{I_1} \tag{2.23}$$

# 3 MATERIALS AND METHODS

## 3.1 MATERIALS

### 3.1.1 Interdigitated electrodes

Interdigitated ENIG electrodes (ENIG: Electroless Nickel Immersion Gold), supplied by Micropress S.A., were used as substrate. They are composed of 18 pairs of 7.9 mm long and 0.1 mm width, with a gap of 0.1 mm between electrode strips (electrodes define an active area of 7.9 mm × 8 mm = 56.8 mm²) mounted on a glass fiber board reinforced epoxy resin (FR4) at thickness 1 mm (Fig. 12).

The resin board (FR4) has low water absorption (<0.1%), it is an insulator (dielectric constant of 4.70) with good mechanical resistance (Young modulus of 24 GPa). According to thermogravimetric analysis, the FR4 does not have considerable mass loss as a consequence of degradation or decomposition, in the range of temperatures between 20 °C and 140 °C.[36,82]

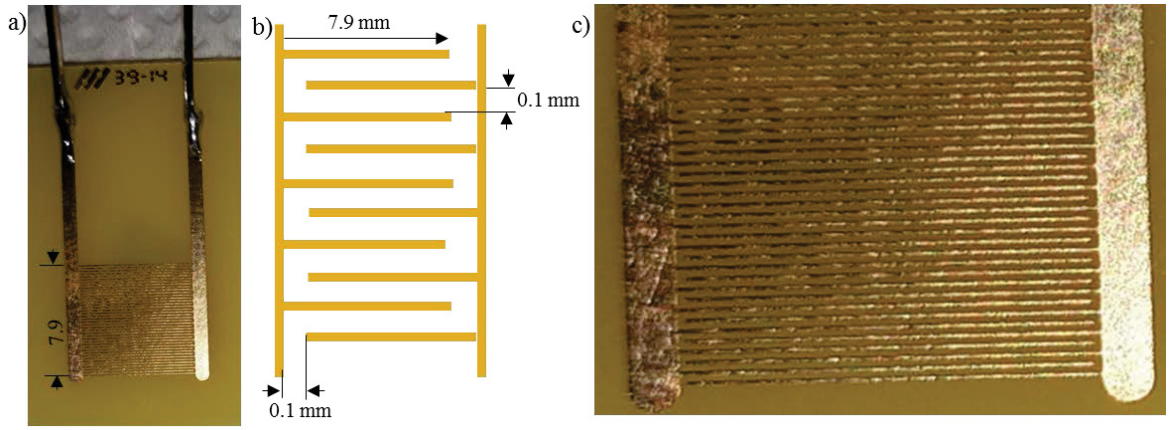


Figure 12 – Photographic images of interdigitated electrodes (a and c) and its scheme (b). In (c), magnification of the active area.

### 3.1.2 Nanomaterials

For this study, nitrogen-doped hollow carbon spheres (N-HCSs), carbon coated GaN (C-GaN) and nitrogen-doped multi-walled carbon nanotubes (A-CNTs) nanostructures were used. They were synthesized and characterized at the *Centre of Excellence in Strong Materials, University of the Witwatersrand (Johannesburg, SA)*, based on a procedure described elsewhere.[83–85] In the sequence, a summary about the nanostructure properties.

*a) Annealed (HCSs) and Nitrogen-doped hollow carbon spheres (N-HCSs)*

Hollow carbon spheres (HCSs) have generated great interests in recent years owing their physico-chemical aspects, applications and low cost production.[86–90] HCSs were synthesized using $SiO_2$ spheres following a procedure reported elsewhere.[83] N-doped HCSs are denoted as either N-HCSs-10 or N-HCSs-50, depending on the fluxing conditions of the nitrogen source during the synthesis (10 or 50 sccm of ammonia gas, respectively).[83] The doping process was performed in a CVD reactor at 600 °C for 1 h. The properties of these N-HCSs are shown in the Table 3 and Fig. 13.

TABLE 3 – Physical and chemical properties of the HCSs and N-HCSs.[83]

| | **Annealed HCSs** | **N-HCS-10** | **N-HCS-50** |
|---|---|---|---|
| **Shell Thickness (nm)** | 25 | 24 | 22 |
| **Decomposition onset temperature (°C)** | 515 | 508 | 492 |
| **$I_D/I_G$ ratio (from Raman spectroscopy)[2]** | 0.51 | 0.53 | 0.72 |
| **Surface areas ($m^2\ g^{-1}$)** | 55.8 ± 0.7 | 81.1 ± 0.5 | 87.6 ± 1.0 |
| **Atomic composition N (%)** | 0 | 0.2 | 0.6 |

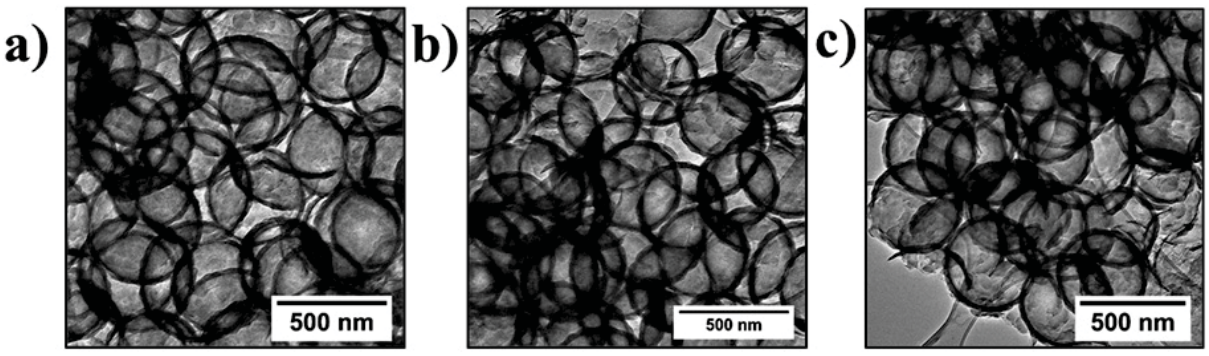


Figure 13 – TEM images of, (a) annealed HCSs, (b) NHCSs-10 and (c) NHCSs-50.[83]

[2]The intensity of the G band ($I_G$) is attributed to the graphitic carbon while the intensity of the D band ($I_D$) indicates the presence of defects or amorphous material within the carbon coating.

*b) Carbon coated GaN (C-GaN)*

In this study, three kind of materials based on GaN were considered: GaN nanoparticles and carbon coated GaN nanostructures (labeled as TA or TN, depending on the gas carrier used during the synthesis process: argon (Ar) or nitrogen (N), respectively). GaN nanoparticles were synthesized using $Ga_2O_3$ and $NH_3$ at 1100 °C. The carbon coated GaN samples were synthesized by chemical vapor deposition (CVD) method using GaN as starting material, at 600 °C with toluene as carbon source and either argon (TA) or nitrogen (TN) as carrier gas. In this study, gallium nitride (GaN) is a wide band gap (3.4 eV at 300 K) semiconductor with wurtzite crystalline structure; the nanoparticles possess a size of 19 nm (in accordance with X-ray diffraction measurement). Additional characteristics are shown in Table 4 and Fig. 14.[84]

TABLE 4 – Some properties of the GaN and C-GaN nanostructures.[84]

| | **GaN** | **C – GaN TA** | **C – GaN TN** |
|---|---|---|---|
| **Decomposition onset temperature (°C)** | 603 | 590 | 475 |
| **$I_D/I_G$ ratio (from Raman spectroscopy)** | - | 0.622 | 0.580 |
| **Surface areas ($m^2\ g^{-1}$)** | 14.2 | 5.9 | 7.4 |

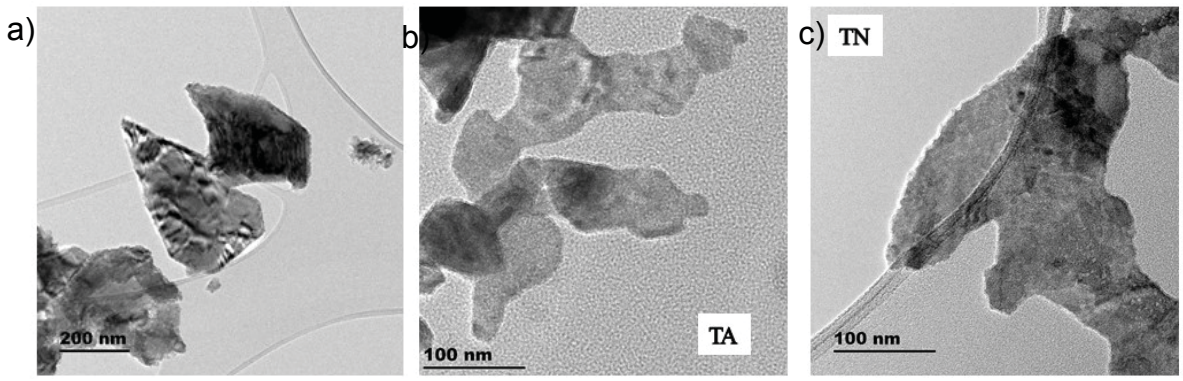


Figure 14 – TEM images of, (a) GaN, (b) C-GaN-TA and (c) C-GaN-TN nanoparticles.[84]

*c) Aligned nitrogen doped multi-walled carbon nanotubes (A-CNTs)*

The aligned nitrogen doped multi-walled carbon nanotubes (A-CNTs) were synthesized by spray pyrolysis procedure (aerosol assisted chemical vapor deposition) using ferrocene into a toluene/acetonitrile solution at 850 °C as described elsewhere.[85] Herein, the carbon nanotubes are denoted as A-CNTx where x = 0 refers to the sample made with toluene as carbon source, x = 0.5 is the sample made with a toluene/acetonitrile solution at the ratio 1:1 and x = 1 refers to the sample made with acetonitrile. A-CNTs are interesting because they are chemically stable, offer excellent mechanical strength, also possess high thermal and electrical conductivity. Additional properties are shown in Table 5 and Fig. 15.[85]

TABLE 5 – Properties of the A-CNTx nanostructures.[85]

| | **x = 0** | **x = 0.5** | **x = 1** |
|---|---|---|---|
| **Shell Thickness (nm)** | 52 ± 11 | 56 ± 39 | 85 ± 49 nm |
| **Decomposition onset temperature (°C)** | 583 | 577 | 574 |
| **$I_D/I_G$ ratio (from Raman spectroscopy)** | 0.55 | 0.83 | 0.89 |
| **Atomic composition N (%)** | 0 | 1.87 | 2.59 |

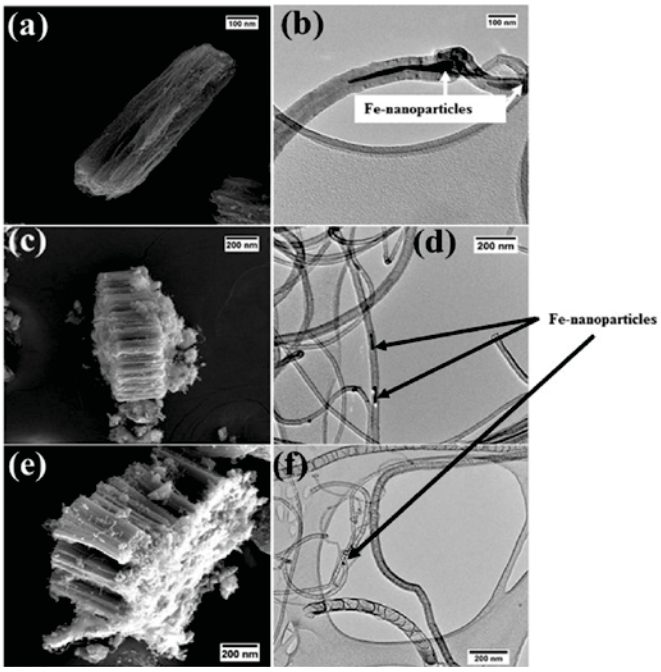


Figure 15 – SEM and TEM images of (a and b) A-CNTx (x = 0), (c and d) A-CNTx (x = 0.5) and (e and f) A-CNTx (x = 1).[84]

### 3.1.3 Chemicals

Surfactant hexadecyltrimethylammonium bromide (CTAB, 98% w/w, Sigma-Aldrich) and analyte ammonium hydroxide, $NH_4OH$ (28% w/w, Fluka) were used as received.

## 3.2 METHODS

### 3.2.1 Preparation of nanomaterial dispersions using a surfactant method

Nanomaterials dispersion were prepared by 2 mg of nanoparticles in 1 mL of deionized water (resistivity >18.2 MΩ $cm^{-1}$). In order to promote a good dispersion of the nanostructures in water, it was assisted by the surfactant CTAB. Dispersions were prepared by adding 4 mg of CTAB into the dispersion with nanostructures, and then, they were sonicated in bath, first for 30 min at 60 °C followed by other 30 min, but at 0 °C. Then, nanostructures/CTAB dispersions were keep for 2 days at 0 °C, this is, below the Kraft temperature[3] of CTAB, (25 °C).[91] The supernatant (~500 µL) of the final dispersion (Fig. 16) was extracted and used in our study for sensor applications.[92]

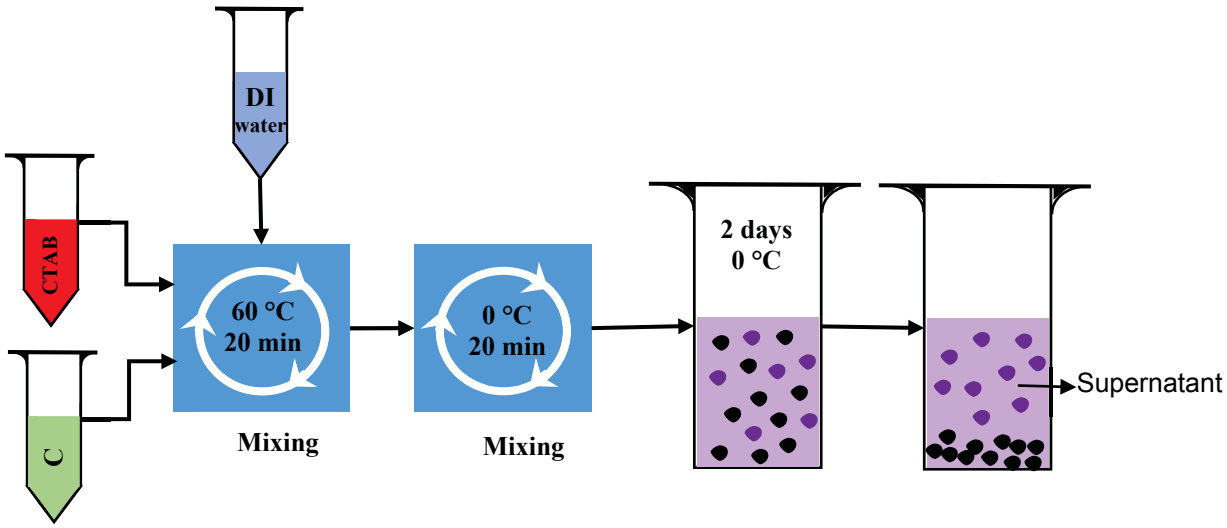


Figure 16 – Scheme of a dispersion with nanostructures.

[3]The temperature below which no micelles are formed.[93]

### 3.2.2 Sensor fabrication and gas sensing measurements

Interdigitated electrodes were sequentially cleaned in acetone, deionized water and isopropyl alcohol by ultrasonication bath for 20 min in each step. The substrates were dried in an oven at 100 °C for 30 min. After that, nanostructures/CTAB dispersion (typically 100 µL) was drop-casted on the active area of the interdigitated electrode. Finally, the sensor device was dried at 100 °C for 30 min, as shown in Fig. 17.[36,52]

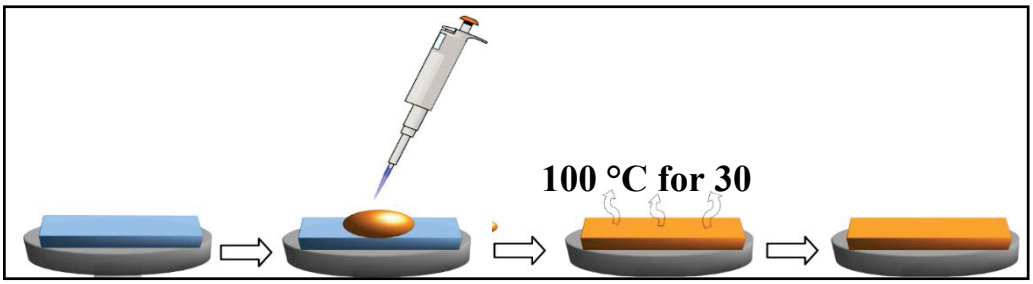


Figure 17 – Scheme of the sensor fabrication.

Regarding to concentration of ammonia and water vapors (C), they were determined from the amount of ammonium hydroxide and water, added to the analysis chamber through the equation:[5,52]

$$C_{\text{ppm}} = \frac{2.46vd}{V_s M_W} \text{x} 10^7 \qquad (2.21)$$

Where $v$ represents the volume (in µL) added to the chamber (in our case 1µL, 2 µL, 3 µL and 4 µL, which correspond to the vapor concentrations shown in Table 6). $V_s$ is the volume (in mL) of the analysis chamber (here: 2000 mL and 2400 mL for HCSs and GaN materials, respectively), $d$ is the density of analyte (in $gmL^{-1}$) and $M_w$ is the molecular weight of analyte in $gM^{-1}$, ($d$ and $M_w$ are listed in the Table A1 of the Appendix 1).

TABLE 6 – Vapor concentration of the analytes calculated using equation 2.21 and $V_s$ = 2000 mL.

| **Analyte** | **Concentration (ppm)** | | | |
|---|---|---|---|---|
| | **1 µL** | **2 µL** | **3 µL** | **4 µL** |
| **Ammonia** | 89 | 178 | 267 | 356 |
| **Water** | 675 | 1350 | 2025 | 2700 |

Concerning to sensors measurements, analytes and binary mixture water:ammonia at 0%, 25%, 50%, 75%, and 100% were dropped into a sealed chamber (properly grounded and unilluminated, Fig. 18), respectively. Measurements were taken after 1 hour, allowing that the analysis chamber reach steady-state conditions. This period of time was determined in a previous work.[36] Sensor response was obtained by resistance measurements, which were carried out using an Agilent 4284A LCR, with an AC signal amplitude of 1 V under dry nitrogen atmosphere.[52]

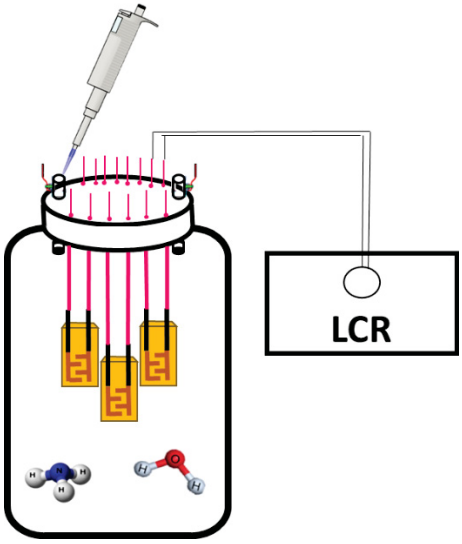


Figure 18 – Scheme of the sensors into the analysis chamber.

Response and recovery time were measured in the same way as described above in the Fig. 18, but using a rotating cap (Fig. 19) which permits to switch the sensor response between the inside of the chamber (exposition to the analyte) and the outside, where the sensor is exposed to dry $N_2$ (inside of a glove box, RH < 20%). This method is described elsewhere.[93]

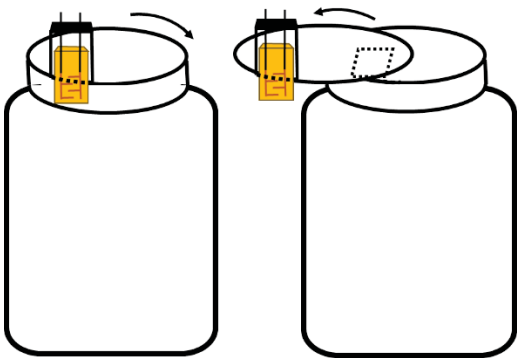

Figure 19 – Diagram showing the sensor inside and outside of the chamber during the transient measurements.[36]

# 4 RESULTS

The results discussed herein are divided into two parts:

1. Nine sensors with different active materials were characterized, by their performance parameters like signal-to-noise ratio, limit of detection and sensitivity, among others. After that, the choice of materials was conducted through evaluation on: (a) the best response to ammonia and poor response to water; (b) good response to water and poor response to ammonia, and lastly (c) material that had best response to both analytes.

2. Once the best sensing materials were selected, the relative concentrations of the analytes (i.e., ammonia and water) are determined by applying the tristimulus methodology.

## 4.1 CHARACTERIZATION OF MATERIALS

The materials characterization was performed by considering the response of the sensors and according to the signal-to-noise ratio (*SNR*) results, together with the best operation frequency for each sensing material. Furthermore, the sensitivity and the limit of detection (*LoD*) results were also used for further characterization.

### 4.1.1 Sensors based on annealed HCSs, N-HCSs-10 and N-HCSs-50

The results based on the ammonia and water sensing ability of the active materials are shown in Fig. 20 and 21. The sensors resistance versus frequency plots for the sensing material composed of the annealed HCSs and N-HCSs are shown in Fig. 20 and 21(a–c), respectively. Moreover, two parameters were used in the determination of the best frequency needed for specific analysis/measurements. The parameters were: (1) high magnitude in the response (see Fig. 20 and 21(a–c)) and (2) the high *SNR* value (see Fig. 20 and 21(d–f)). However, the responses and *SNRs* were not simultaneously high and/or the same for all sensors and analytes. Hence, it was not possible to identify a single frequency that can be used for specific analysis/measurements. Therefore, the values presented in Table 7 are the values of sensor performance at the best operating frequency.

The resistance versus concentration plots are shown in Fig. 20 and 21(g–i), revealing the detection of ammonia and water. This is shown by the increase in resistance with the analyte

concentration. The sensor responses ($\Delta R/R_0$) are presented in Fig. 20 and 21(j–l); they were further used to calculate the sensitivity (see Table 7). This was confirmed that in all cases, the sensors response increased with increasing concentration of the analyte.

The kinetically controlled states of the different sensing devices possibly promote the differences in the behavior, as well as the shape of the baseline (this is, at zero concentration) in the resistance-frequency curves for the sensors. This effect can be due to the sensing material dispersion and the sensors film thicknesses, given that different sensors were used for the detection of each analyte. This suggests that it is possible for certain films (giving a specific shape to the resistance-frequency plot) to be better suitable for detecting specific analytes.

Saturation of the sensors towards high concentrations of different analytes was noted in some cases. When it occurred, the sensitivity was estimated by using only the three lowest concentration values for the analysis.

Table 7 – Frequency *f*, determined limit of detection (*LoD*) and sensitivity *S* for ammonia and water detection in sensors based on annealed HCSs and N-HCSs.

| **Analyte** | **Material** | **Frequency (kHz)** | ***LoD*** **(ppm)** | **Sensitivity ($ppm^{-1}$)** |
|---|---|---|---|---|
| **Ammonia** | Annealed HCSs | 6 | 19 | $5.9 \times 10^{-4}$ |
| | N-HCSs-10 | 3 | 6 | $5.2 \times 10^{-4}$ |
| | N-HCSs-50 | 1 | 40 | $1.4 \times 10^{-4}$ |
| **Water** | Annealed HCSs | 10 | 62 | $7.3 \times 10^{-3}$ |
| | N-HCSs-10 | 20 | 30 | $2.4 \times 10^{-3}$ |
| | N-HCSs-50 | 10 | 7 | $5.6 \times 10^{-4}$ |

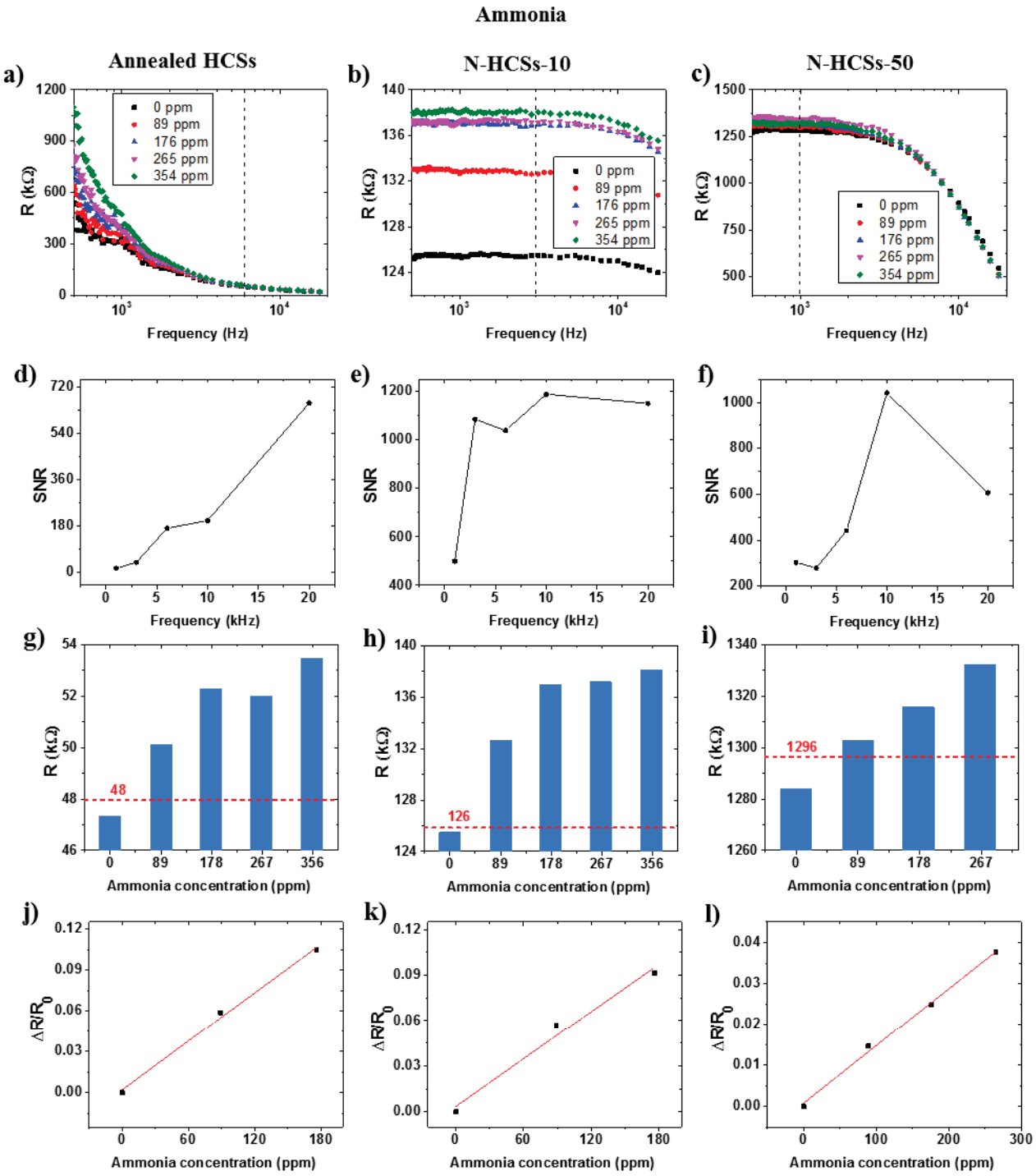


Figure 20 – Data set for sensors based on annealed HCSs, N-HCSs-10 and N-HCSs-50, when exposed to ammonia, are presented in the first, second and third columns, respectively. (a–c) Sensor resistance dependence on frequency; dashed line indicates the optimum operating frequency; (d–f) sensor signal to noise ratio (*SNR*) as a function of frequency at 0 ppm; (g–i) resistance as a function of analyte concentration; the dotted red line indicates the estimated *LoD* resistance of the corresponding sensor and (j–l) response of the sensor versus analyte concentration.

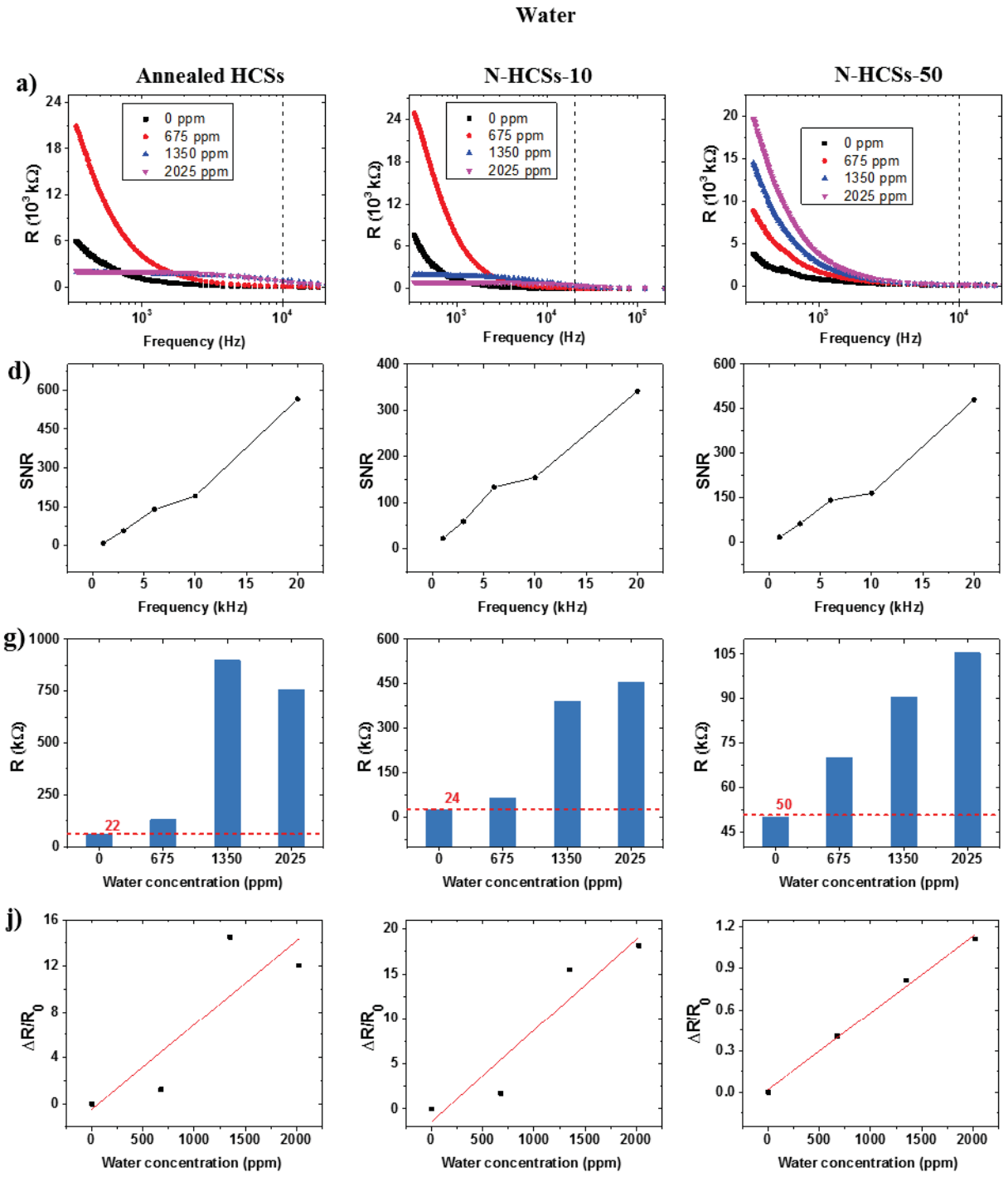


Figure 21 – Data set for sensors based on annealed HCSs, N-HCSs-10 and N-HCSs-50, when exposed to water, are presented in the first, second and third columns, respectively. (a–c) Sensor resistance dependence on frequency; dashed line indicates the optimum operating frequency; (d–f) sensor signal to noise ratio (*SNR*) as a function of frequency at 0 ppm; (g–i) resistance as a function of analyte concentration; the dotted red line indicates the estimated *LoD* resistance of the corresponding sensor and (j–l) response of the sensor versus analyte concentration.

The sensitivity of the active material can be changed depending on the density of the charge carriers. The increase in the density of negative charge carriers would lower the ammonia sensitivity in the case of N-HCSs (as shown in Table 7). This is because the ammonia molecules serve as electron donors while the presence of nitrogen-containing groups on the N-HCSs surface provides an electron rich HCSs environment.

Therefore, when looking at the case of annealed HCSs (i.e. absence of nitrogen-containing groups), this material would be suitable to accept electrons through active accepting sites for the ammonia molecules, resulting in the higher ammonia sensitivity.

The obtained results further suggest that the annealed HCSs gave a higher limit of detection for water as compared to the N-HCSs (see Table 7). This can be due to the presence of structural defects introduced by nitrogen heteroatoms in the N-HCSs surface that allows the interaction of the nitrogen-containing groups with the water molecules. It was also noted that the sensitivity (i.e. response as a function of analyte concentration) of annealed HCSs was higher as compared to the N-HCSs, meaning that the response and recovery towards the water molecules was faster. Furthermore, this could be due to the use of a pure carbon surface (as confirmed by the TGA data),[83] the presence of fewer oxygenated groups on the surface (as confirmed by the XPS data)[83] and hence a weaker interaction of the annealed HCSs surface with water molecules. The lower sensitivity towards water molecules obtained for the N-HCSs can be due to the presence of stronger interactions between the different oxygen and nitrogen containing groups with the water molecules.

Table 8 revealed that the increase in nitrogen contents in the HCSs decreased the sensitivity for all analytes when it was determined at the same frequency (i.e. 6 kHz for all the sensors). Moreover, the annealed HCSs exhibited higher sensitivities towards ammonia and water vapors as compared to the all N-HCSs. The N-HCSs-50 showed the lowest sensitivity towards water as compared to the N-HCSs 10. This suggest that the use of ammonia and heat treatment when synthesizing N-HCSs collaborated in limiting active sites for the water vapor detection in the N-HCSs based sensors. Furthermore, the amorphous carbon was removed by heating at 600 °C in ammonia while incorporating nitrogen defects on the HCSs surface. This behavior can be good for application in sensor arrays. It can be used for analyte discrimination in humid environments since it can allow for the separation of the water contribution to the different sensors's responses.

The N-HCSs exhibited lower ammonia sensitivity, which suggests that the lower presence of O–N, O–C=O, C–N and C–O functional groups on the N-HCSs surface could impact on their vapor sensing properties, as suggested by XPS results reported elsewhere.[83]

Table 8 – Sensitivity to different analytes for annealed HCSs, N-HCSs-10 and N-HCSs-50 based sensors at operation frequency of 6 kHz.

| | Sensitivity ($ppm^{-1}$) | | |
|---|---|---|---|
| **Analyte** | **Annealed HCSs** | **N-HCSs-10** | **N-HCSs-50** |
| **Ammonia** | $5.9 \times 10^{-4}$ | $1.4 \times 10^{-4}$ | $1.3 \times 10^{-4}$ |
| **Water** | $3.0 \times 10^{-2}$ | $4.0 \times 10^{-2}$ | $3.0 \times 10^{-3}$ |

### 4.1.2 Sensors based on carbon coated GaN (C-GaN)

The sensing properties of GaN, C-GaN TN and C-GaN TA nanoparticles were evaluated for both ammonia and water. The obtained results are summarized and presented in the Figs. 22 and 23, with typical measurements of resistance as a function of analyte concentrations as well as frequency (see Fig. 22 and 23(a-c)). It was noticed that in all cases, the resistance decreased with increasing frequency, with similar trend in the sensitivity due to its dependence with the sensor response, in accordance with equation 2.10. This behavior follows the charge transport in disordered materials.[94,95] At long time scales (low frequencies) charge carriers follow the alternating electric field, travelling relative long distances and overcome potential barriers with several heights (some of these charges could be trapped on the nanostructure surface). At shorter time scales (high frequencies > 20 kHz) charge carriers are not able to follow the oscillating signal, restricting their movement to short distances (e.g. only inside the nanostructure) which decrease the electric resistance because only the smaller barriers are surpassed and an increase in the conductivity is observed.

Similarly to that was observed in HCSs based sensors, the resistance versus frequency plots reveal different behaviors for the analyte concentration (i.e. 0 ppm) for different devices. This is possibly due of the experimental differences in the material deposition (i.e. dispersion and film thickness). The SNR results further reveal an increase with frequency as general trend, as shown in Figs. 22 and 23(d-f). Thus, the optimal sensor frequency operation lies at intermediate values, one that equilibrates sensor response and the *SNR*. However, a single

optimum operating frequency was not achieved for the whole set of sensors and analytes (see Table 9). The optimal frequency selected for water was 3 kHz whereas that of ammonia varied between 3 and 6 kHz depending on the sensing materials, as shown in the Table 9. Different operation frequencies were necessary for the observed sensor responses (see Fig. 22 and 23(g-i)). The sensitivities of the sensors were further calculated by assuming a linear dependence and using the results in Fig. 22 and 23(j-l). At higher analyte concentrations some sensors tend to saturation (e.g. for C-GaN TN based sensor). In those cases of higher analyte concentrations, the sensitivity was calculated with the three lowest values of the concentrations.

Table 9 – Frequency *f*, limit of detection (*LoD*) and sensitivity *S* for the detection of ammonia and water in sensors based on GaN, C-GaN TN and C-GaN TA.

| **Analyte** | **Material** | **Frequency (kHz)** | ***LoD*** **(ppm)** | **Sensitivity ($ppm^{-1}$)** |
|---|---|---|---|---|
| **Ammonia** | GaN | 3 | 43 | $7.7 \times 10^{-4}$ |
| | C- GaN TN | 6 | 3.4 | $3.7 \times 10^{-3}$ |
| | C- GaN TA | 6 | 6.8 | $1.1 \times 10^{-3}$ |
| **Water** | GaN | 3 | 744 | $1.1 \times 10^{-4}$ |
| | C- GaN TN | 3 | 250 | $1.3 \times 10^{-4}$ |
| | C- GaN TA | 3 | 295.8 | $1.6 \times 10^{-3}$ |

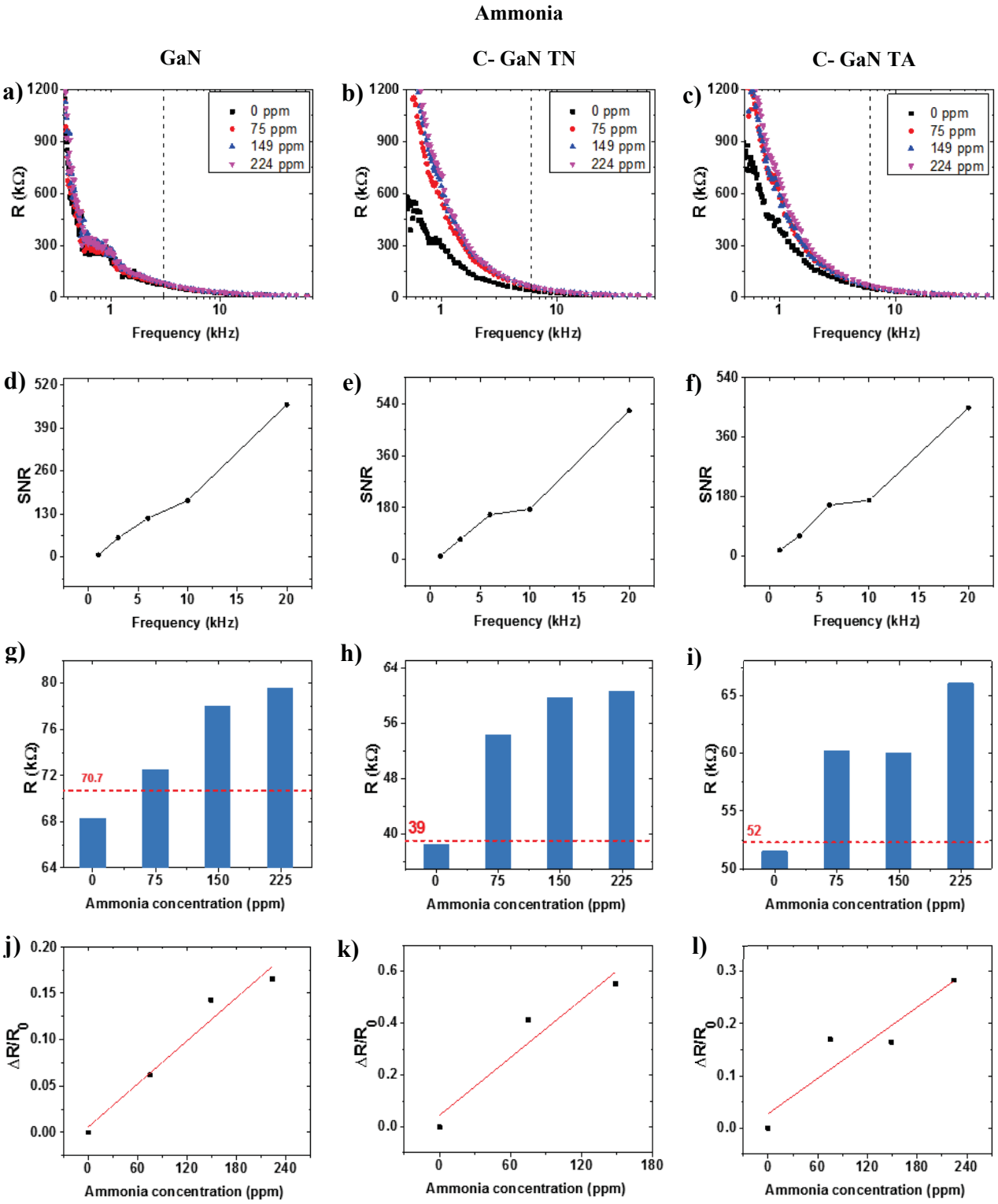


Figure 22 – Data set for sensors based on GaN, C-GaN TN and C-GaN TA, when exposed to ammonia, are presented in the first, second and third columns, respectively. (a–c) Sensor resistance dependence on frequency; dashed line indicates the optimum operating frequency; (d–f) sensor signal to noise ratio (*SNR*) as a function of frequency at 0 ppm; (g–i) resistance as a function of analyte concentration; the dotted red line indicates the estimated *LoD* resistance of the corresponding sensor and (j–l) response of the sensor versus analyte concentration.

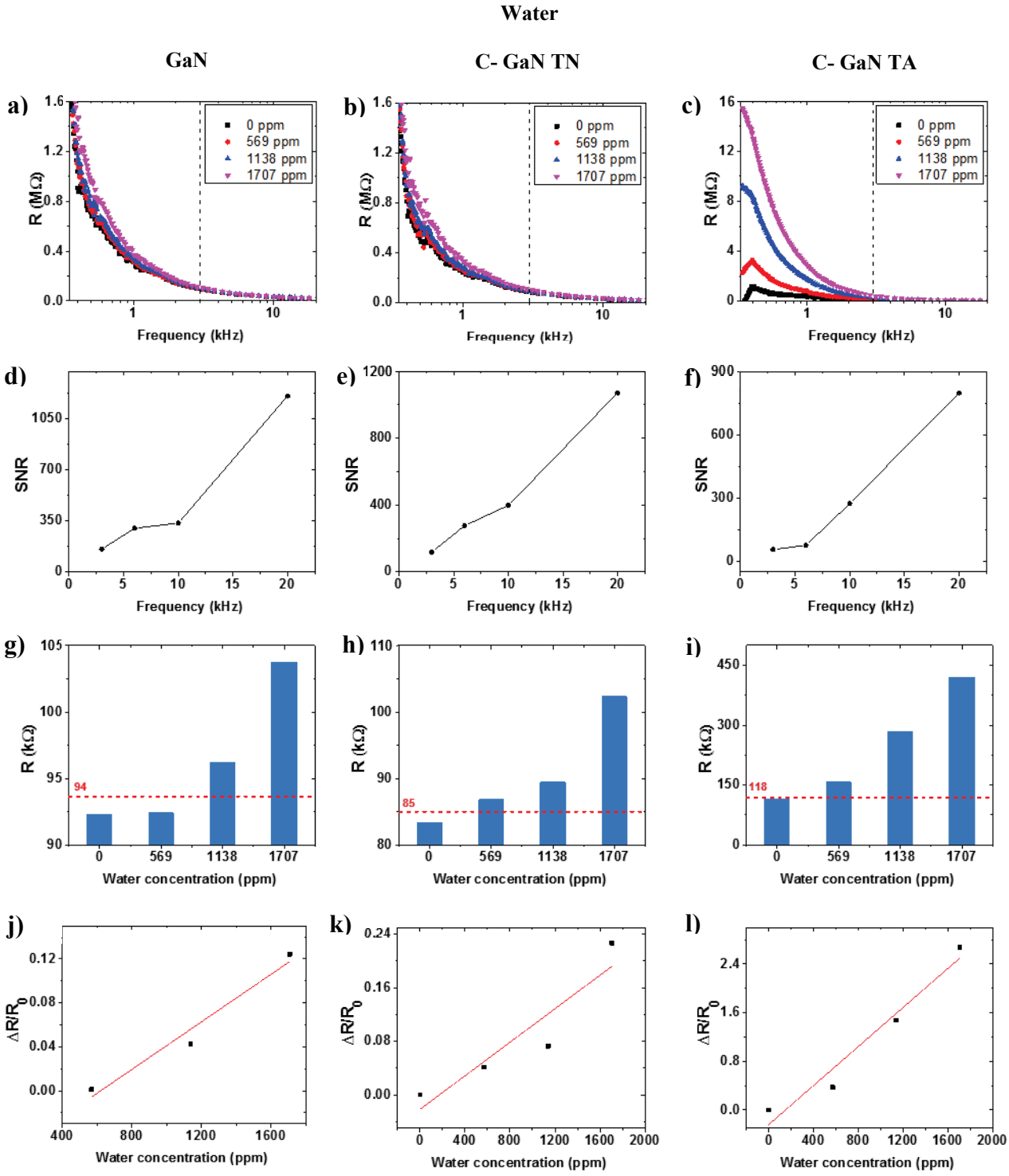


Figure 23 – Data set for sensors based on GaN, C-GaN TN and C-GaN TA, when exposed to water, are presented in the first, second and third columns, respectively. (a–c) Sensor resistance dependence on frequency, dashed line indicates the optimum operating frequency; (d–f) sensor signal to noise ratio (*SNR*) as a function of frequency at 0 ppm; (g–i) resistance as a function of analyte concentration, the dotted red line indicates the estimated *LoD* resistance of the corresponding sensor and (j–l) response of the sensor versus analyte concentration.

Since for both the analytes it was observed that resistance and the sensors response increased together with concentration, it can be affirmed that the sensors present similar behavior as compared to sensors based on p-type semiconductors when exposed to reducing organic volatile gases.[12,62,83,96–98] In the case of GaN, it can be either n- or p–type semiconducting material, depending on the doping process.[99] The characteristics of the synthesized undoped material considered in this study would be given by the defects introduced during the synthesis process, which are likely to be nitrogen vacancies. These vacancies can act as sorption sites for gas molecules on the surface or other contaminants,[96] giving rise to possible shallow acceptor sites.[36,100–107] Hence, it is suggested that the GaN can behave as a p–type semiconducting material during the analysis.

The sensitivities and *LoDs* values for both the analytes considered in this study are shown in the Table 9, at optimized operation frequencies. These results show that the sensitivity of C-GaN based sensors is higher for ammonia, with lower *LoD* values.

Ammonia is a reducing agent with a lone electron pair (i.e. an electron donor) and thus, it can transfer negative charges to GaN, being responsible for the resistance increase with analyte concentration. Furthermore, the captured electrons by nitrogen vacancy sites can also lead to an increase in resistance, since GaN can be regarded as a p-type semiconductor.

When exposing the carbon-coated GaN (C-GaN) nanoparticles to an analyte, there is a reduction in the interacting GaN with the analyte due to the carbon atoms on the surface, as expected, and particularly, the interaction between the defects in GaN and the analyte is diminished, whereas there is a significant decrease in surface area (table 4). Therefore, the interaction now occurs in its majority with carbon containing sites. The carbon could be entering also as an unintentional impurity in GaN during the coating process, through carbon-nitrogen substitution, acting as a p-type dopant. Thus, C-GaN nanoparticles preserve their p-type nature.

Having the p-type behavior of the material, the sensitivity increase can be related to the increase in adsorption sites even though the material has lower surface area. By increasing carbon coating, such as in C-GaN TA nanoparticles, there is a possible further reduction on surface area. This can diminish the exposure of sorption nitrogen containing sites leading to a reduction on sensitivity towards the ammonia molecules. Additionally, more carbon atoms can offer surfaces for conduction that may favor the charge interaction between analyte molecules and sensing material.[83]

According to the results in Table 9, (i.e. for water), the most sensitive material was C-GaN TA followed by C-GaN TN and GaN, respectively. As Reti et al[108,109] and Tsai et al[110] reported that water has a multiple effect on surface material, it can be suggested that the similar occurrence takes place with the GaN material. Firstly, the adsorbed water molecules can inject electrons into the solid sensing material, increasing the sensors resistance. The surface hydroxyl groups are then given out which can also interact with the surface atoms leading to resistance increase as well. The carbon-coated GaN nanoparticles (C-GaN TA and C-GaN TN) leads to a substitution of GaN by carbon interaction sites. The adsorbed water molecules serve as electron donors, which further increase the resistance of the sensing material. However, it must be noted that with enough water molecules in the reaction system, the adsorbed water molecules may be ionized to produce hydronium anions which act as positive charge carriers, causing a decrease in the resistance.[111] By considering the most stable configuration for the interaction water–GaN (or C-GaN), the charge transfer to the sensing material is not so effective compared to ammonia, for example as explained by Yong et al.[112] It means the band structures in GaN or C-GaN TN are less affected, leading to their lower sensitivity to water, when compared to C-GaN TA based sensor.

Furthermore, the performance of the C-GaN based sensors was evaluated at the same frequency (see Table 10). The similar behavior to that seen previously in the results contained in Table 9 was observed and it can be seen that highly sensitive material to ammonia is C-GaN TN whereas C-GaN TA based sensors present high response to water and ammonia. It is worth remembering that for a particular device, the *SNR* is low only when it is exposed to some analytes. Hence, a single operation frequency was not considered in the earlier discussion.

Table 10 – Sensitivity to different analytes for GaN, C-GaN TN and C-GaN TA based sensors at the operation frequency of 3 kHz.

| **Analyte** | **GaN** | **C- GaN TN** | **C- GaN TA** |
|---|---|---|---|
| **Ammonia** | $7.7 \times 10^{-4}$ | $5.2 \times 10^{-3}$ | $1.6 \times 10^{-3}$ |
| **Water** | $1.1 \times 10^{-4}$ | $1.3 \times 10^{-4}$ | $1.6 \times 10^{-3}$ |

The measurements were repeated by using two new sensors with new dispersions of the nanomaterials, checking the repeatability of the responses, e.g. the Fig. 24 shows similar sensitivities for water in sensors based on GaN:

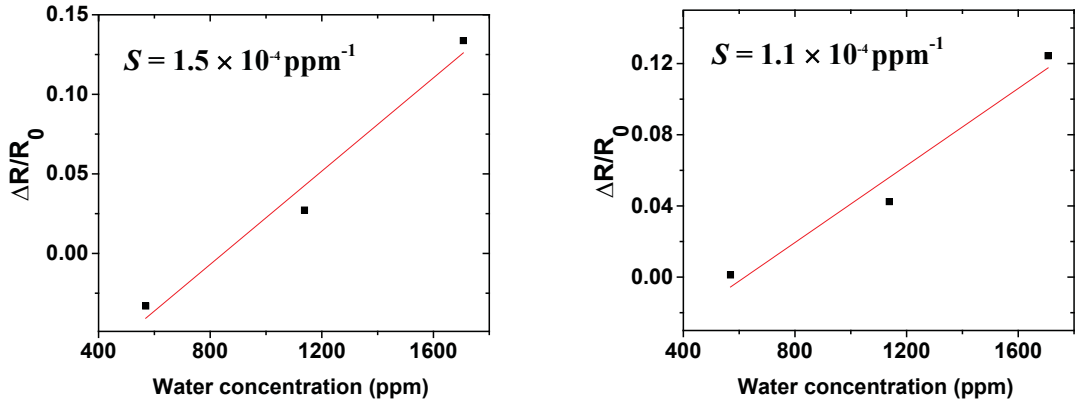


Figure 24 – Comparison of the sensitivities (*S*) for different sensors based on GaN when exposed to water vapor.

### 4.1.3 Aligned nitrogen doped multi-walled carbon nanotubes (A-CNTs)

The devices based on A-CNTs (x = 0, x = 0.5, x = 1) showed no response to ammonia and water, because of the low signal-to-noise ratio, a trend could not be established for the performance of these materials towards sensing of ammonia and water vapors.

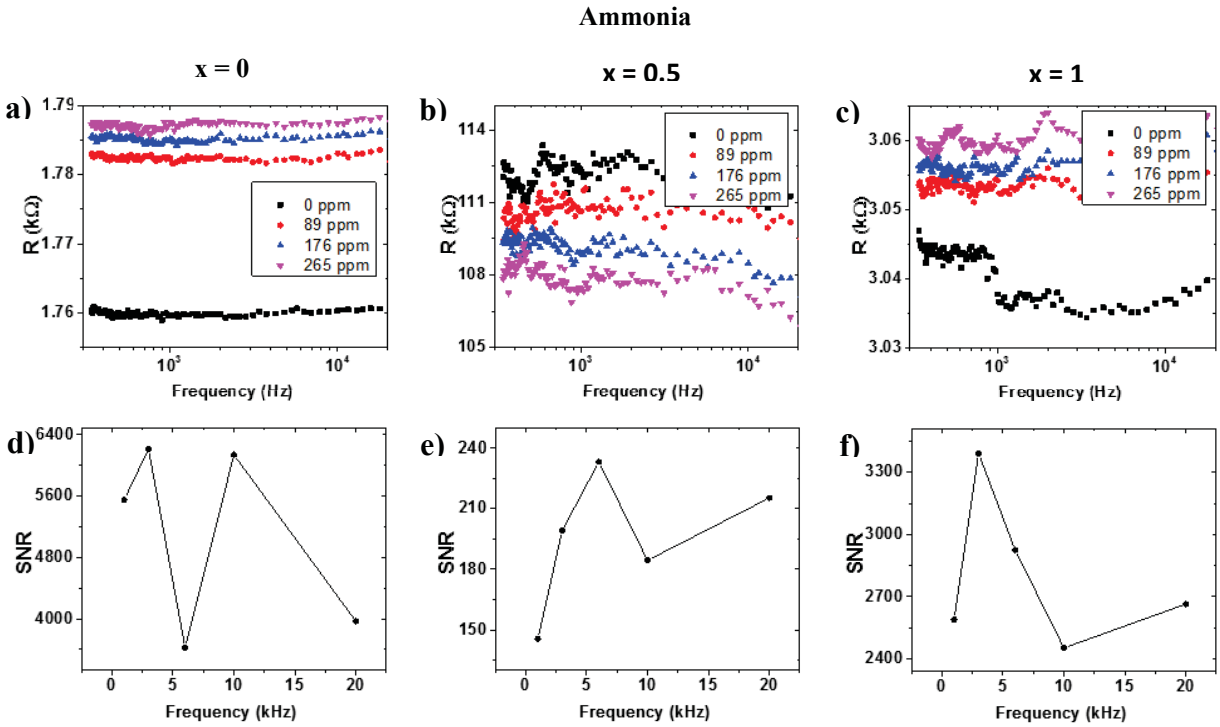


Figure 25 – Data set for sensors based on A-CNTx (x = 0), A-CNTx (x = 0.5) and A-CNTx (x = 1) nanoparticles, when exposed to ammonia, are presented in the first, second and third columns, respectively. (a–c) Sensor resistance dependence on frequency; (d–f) sensor signal-to-noise ratio (*SNR*) as a function of frequency at 0 ppm.

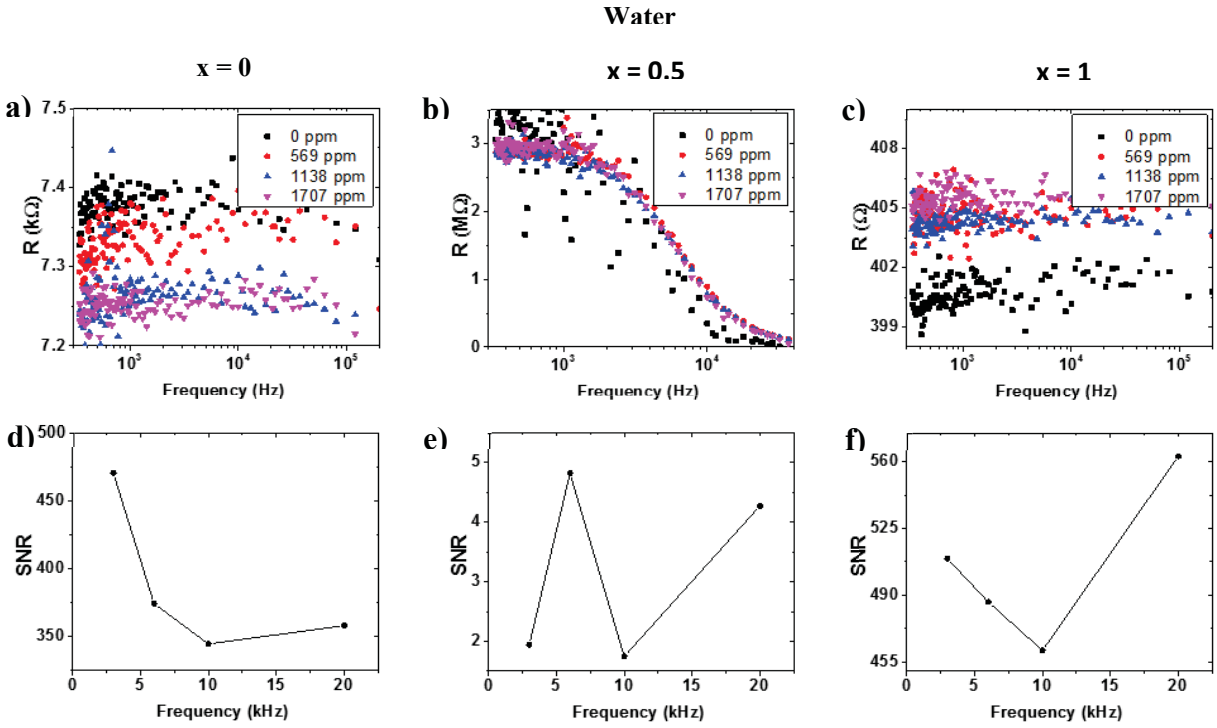


Figure 26 – Data set for sensors based on A-CNTx (x = 0), A-CNTx (x = 0.5) and A-CNTx (x = 1) nanoparticles, when exposed to water, are presented in the first, second and third columns, respectively. (a–c) Sensor resistance dependence on frequency; (d–f) sensor signal-to-noise ratio (*SNR*) as a function of frequency at 0 ppm.

### 4.1.4 Comparison of results with literature

Figure 27. Compares the responses measured at room temperature in this work, which are similar to those previously reported by Mutuma (with HCSs/PVP as sensing material, at 40°C) and higher than those showed in the Table 2 (except for RGO-PANI reported by Huang et al[62]) for different nanomaterials at room temperature.

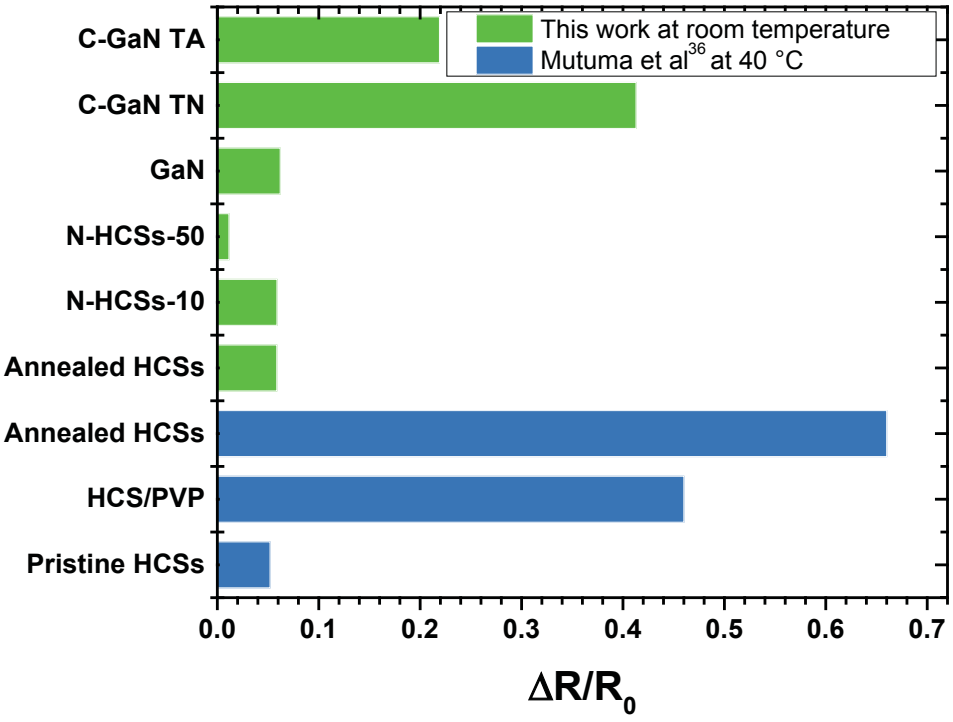


Figure 27 – Comparison of ammonia sensors based on different materials at 74 ppm

### 4.1.5 Material selection

For material selection, the Fig. 28 compares the relative responses of the different materials evaluated above, in order to know which ones, have greater affinity towards ammonia and water at 3 kHz.

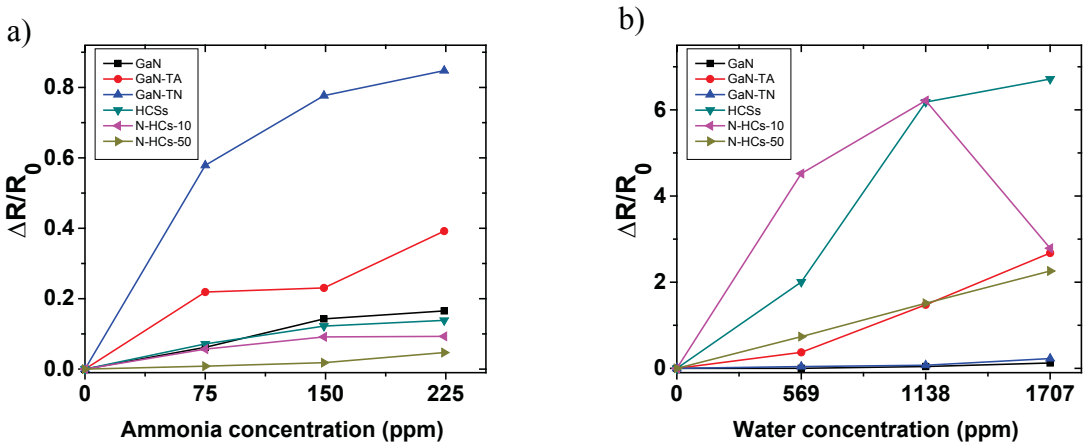


Figure 28 – Comparison between sensors based on N-HCSs and C-GaN nanoparticles. Sensor responses when exposed to ammonia (a) and water (b) as a function of the analyte concentration, at 3 kHz.

Fig. 29 shows the nanostructured materials that were choose because of their different response to the same analyte: GaN-TN presented the highest response to ammonia and lowest response to water, unlike HCSs which had the highest response to water, but low response to ammonia, and finally, N-HCSs-50 had an intermediate response.

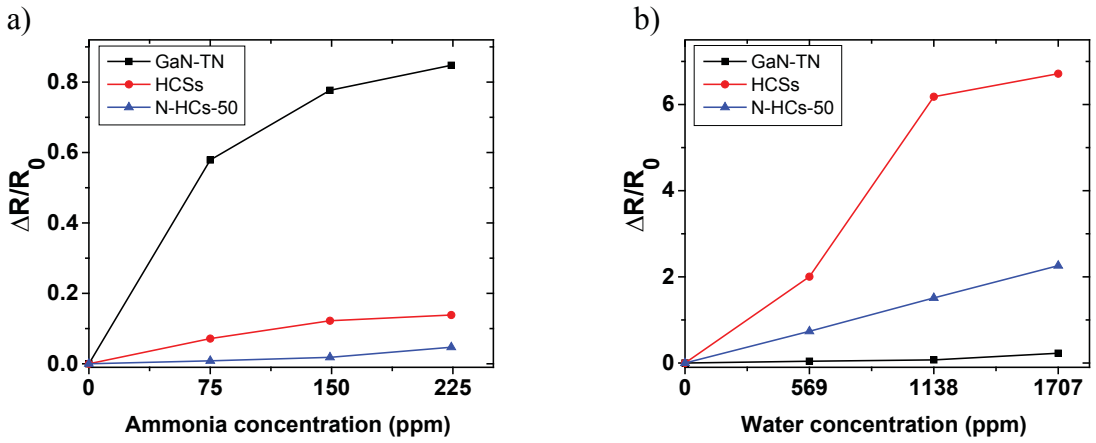


Figure 29 – Response of the sensors based on GaN-TN, HCSs and N-HCs-50 versus analyte concentration, at the same frequency of 3 kHz, when exposed to ammonia (a) and water (b).

Fig. 30 compares the sensitivity of the selected materials in Fig. 29. As can be appreciated, the sensitivities follow the same pattern observed in the sensor responses (Fig. 29).

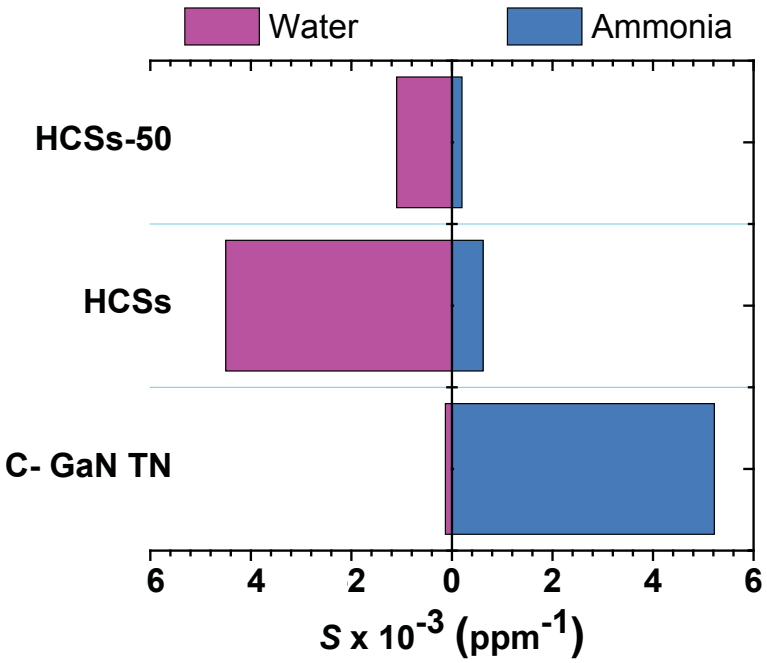


Figure 30 – Comparison of the sensitivities for sensors based on the selected materials, at the operating frequency of 3 kHz.

Once the active materials and best operating conditions for the sensors were determined, ammonia sensing in a humid environment can be evaluated through the tristimulus methodology.

### 4.1.6 Response and recovery time

Fig. 31 shows the response and recovery times for ammonia and water respectively. Ammonia sensor based on C-GaN TN and water sensor based on HCS showed higher signal to noise ratio than the other sensors. Which confirm the affinity that these materials have towards ammonia and water as is shown in Fig. 30.

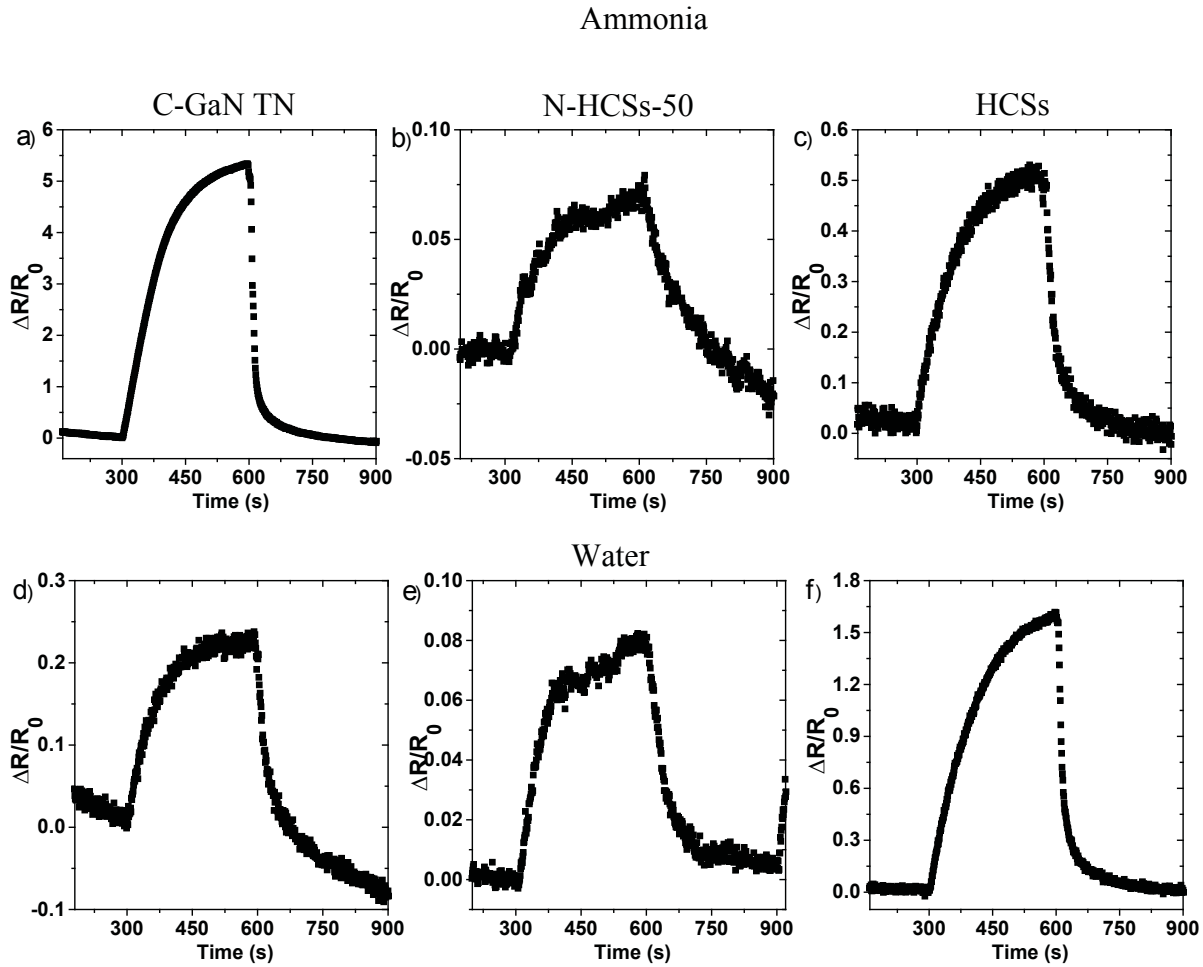


Figure 31 – Response-recovery time for ammonia and water at 178 and 1350 ppm, respectively, based on (a and d) C-GaN TN, (b and e) N-HCSs-50 and (c and f) HCSs.

The repeatability of the sensor, this is, response cycles without significant variation, can be verified by performing several measurement cycles. The figure 32 shows the repeatability of the response-recovery time of the sensor based on N-HCSs-50 for water.

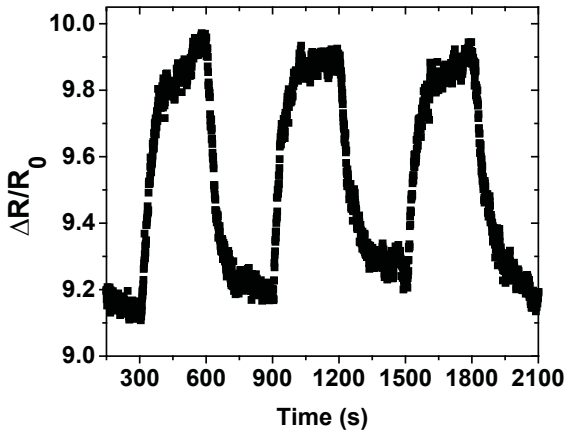


Figure 32 – Repetitive response-recovery times for the sensor based on N-HCSs-50 when exposed to water vapor.

The response and recovery time values are summarized in the table 11. The shortest response and recovery times for ammonia and water were observed in the case of C-GaN TN and HCS sensors, respectively. The ammonia absorption rate of the C-GaN TN surface was higher than that of the HCSs resulting in shorter response times.

Table 11 – Response ($t_{resp}$) and recovery ($t_{recov}$) time for sensors based on C-GaN TN, N-HCSs-50 and HCSs.

| **Analyte** | **Sensor** | **$t_{resp}$ (s)** | **$t_{recov}$ (s)** |
|---|---|---|---|
| Ammonia | C-GaN TN | 95 | 48 |
| | N-HCSs-50 | 115 | 164 |
| | HCSs | 122 | 63 |
| Water | C-GaN TN | 89 | 67 |
| | N-HCSs-50 | 82 | 86 |
| | HCSs | 85 | 49 |

## 4.2 TRISTIMULUS ANALISYS

The Fig. 33 shows the comparison of the responses for the binary mixture water/ammonia, using the predicting model and experimental results. The curve is obtained

from the equation 2.20 based on the sensitivities of the three sensors (where the subscripts 1, 2 and 3 stands for C-GaN TN, N-HCSs 50 and HCSs, respectively) to each pure analyte separately (predictive model). The blue, red and black points are obtained based on the responses of the three sensors for the relative water concentrations 0%, 25%, 50%, 75% e 100% of the binary mixture.

The tristimulus analysis allows to know qualitatively the pattern related to changes in the relative concentration of analytes, however, at high analyte concentrations (> 1000 ppm) the responses dislocated from the predictive pattern. It was also reported by Rodriguez and Mutuma,[36,52] and it is related with possible preferred interactions between some analytes and the active layer or with the formation of complexes between the analytes of the system. Despite the experimental data do not follow the expected pattern; it is possible to differentiate the corresponding responses to different ammonia and water concentrations because they do not overlap.

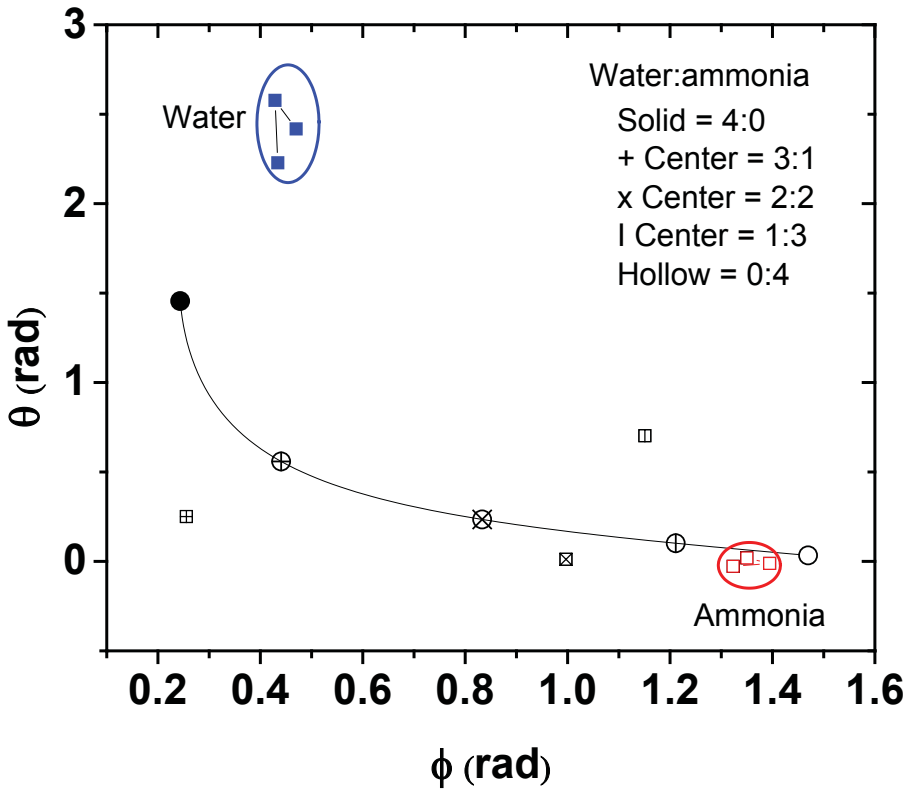


Figure 33 – Tristimulus analysis for the binary mixture water:ammonia at 0%, 25%, 50%, 75%, and 100%. The black curve indicates the predicted response by the eq. 2.20, circles indicate the predicted responses at the specified relative concentrations. Square points are the experimental responses at the specified relative concentrations obtained from the eqs. 2.22 and 2.23 Blue and red data are the experimental responses to pure analytes.

# 5 CONCLUSIONS

The fabrication and characterization of sensors based on HCSs (N-HCSs), GaN (C-GaN) and A-CNTs were investigated when exposed to ammonia and water. Electrical resistance measurements as a function of both frequency and analyte concentration were performed to determine the best *LoD* and sensitivity values.

All the nanostructures considered in this study showed potential applications as active materials in chemical vapor sensors, particularly for ammonia and water. Regarding to N-HCSs-50, they exhibited lower sensitivity to water ($3.0 \times 10^{-3}$ ppm$^{-1}$) in comparison to HCSs ($3.0 \times 10^{-2}$ ppm$^{-1}$), which means there is a limiting factor on water detection coming from the post-nitrogen doping and thermal treatment during the synthesis process. In other words, the N-HCSs are convenient for operating in a stable manner in humid environments whereas they are sensing other volatile compounds.

What concerns to GaN, C-GaN TN and C-GaN TA nanoparticles, they responded to both ammonia and water. C-GaN TN got the higher sensitivity for ammonia ($3.7 \times 10^{-3}$ ppm$^{-1}$), whereas the lower one was achieved for water ($1.3 \times 10^{-4}$ ppm$^{-1}$).

The devices based on A-CNTs could not be characterized for the analytes used. This can be attributed to the deposition method of the nanotubes, this is, it was not adequate.

Response and recover times were stable, indicating that the devices could be used in real applications with the advantage of being able to be used at room temperature. Additionally, these times (as shown in the Table 11) were similar to those reported by previous authors (Mutuma 2017).

Considering linear and different response to the same analyte, three sensors were selected to apply the tristimulus analysis methodology: C-GaN TN, annealed HCSs and N-HCSs-50. This simple pattern recognition technique based on a generalized tristimulus analysis makes possible to distinguish simultaneously the relative concentrations of water and ammonia in the binary mixture by using a set of three different sensors.

During the master's studies, the sensors were also characterized when exposed to methanol, lactic acid, acetone, toluene and chloroform. These results were published in scientific journals and they are not included here because they are beyond the topic of this dissertation.

## 5.1 FUTURE DIRECTIONS

In the following, some proposed future and potential studies, for the improvement of this project:

1. Evaluate other materials (like other carbon allotropes and related hybrid compounds, including metal oxides) and different analytes as well as preparation methods. These methods must be focused in the obtaining of high responses and low noise signal. Regarding to the materials, they must be selective to the analytes of interest, allowing in this manner the use of the tristimulus methodology.
2. In the case of the study of sensors based on A-CNTs, it would be interesting to investigate other conditions in the dispersion preparation, for example, several A-CNTs concentrations, temperatures, other surfactants (anionic, cationic or non-ionic) and so on.
3. Extend the tristimulus analysis (a three-sensors method) to n-stimuli methodology (a n-sensors system) by developing the mathematical models necessary for this purpose, taking into account that n-stimuli would not have a graphical representation in space, compared to the tristimulus analysis that has a three-dimensional representation.
4. Use a set of n-sensors to detect a greater amount of analytes and bring the study closer and closer to applications required in the different fields of action.

## REFERENCES


1 B. R. Eggins, *Chemical Sensors and Biosensors*, 2004.
2 E. T. Powner and F. Yalcinkaya, *Sens. Rev.*, 1995, **15**, 19–22.
3 A. H. Deshpande, J. M. Weldode and J. S. Pise, *Int. J. Manag. Technol. Eng.*, 2018, **8**, 1403–1408.
4 C. W. Na, J. H. Kim, H. S. Woo, A. Gupta, H. K. Kim and J. H. Lee, *Sensors Actuators, B Chem.*, 2018, **255**, 1671–1679.
5 W. Chen, S. Laiho, O. Vaittinen, L. Halonen, F. Ortiz, C. Forsblom, P. H. Groop and M. Lehto, *J. Breath Res.*, 2016, **10**, 036011-036011–11.
6 B. Timmer, W. Olthuis and A. Van Den Berg, *Sensors Actuators, B Chem.*, 2005, **107**, 666–677.
7 R. Geetha and V. Gayathri, *Int. J. Nanosci.*, 2017, **15**, 1–6.
8 A. N. Parinaz Seifaddini, Roghayeh Ghassempour, Mohammad Ramezannezhad, *Mater. Res. Express*, 2019, **6**, 1–14.
9 N. D. Hoa, N. Van Quy, Y. Cho and D. Kim, *Sensors Actuators B Chem.*, 2007, **127**, 447–454.
10 Z. Ben Aziza, Q. Zhang, D. Baillargeat, Z. Ben Aziza, Q. Zhang and D. Baillargeat, *Appl. Phys. Lett.*, 2014, **105**, 254102-254102–4.
11 J. Wu, K. Tao, J. Miao and L. K. Norford, *Appl. Mater. Interfaces*, 2015, **7**, 27502−27510.
12 Y. Wang, L. Zhang, N. Hu, Y. Wang, Y. Zhang, Z. Zhou, Y. Liu and S. Shen, *Nanoscale Res. Lett.*, 2014, **9**, 1–12.
13 J. L. Johnson, A. Behnam, Y. An, S. J. Pearton, A. Ural, J. L. Johnson, A. Behnam, Y. An, S. J. Pearton and A. Ural, *J. Appl. Phys.*, 2011, **109**, 124301-124301–7.
14 E. C. Mattson, K. Pande, M. Unger, S. Cui, G. Lu, M. Weinert, J. Chen and C. J. Hirschmugl, *J. Phys. Chem.*, 2013, **117**, 10698−10707.
15 P. Teerapanich, M. Tay, Z. Myint, C. M. Joseph and G. L. Hornyak, *Trans. Nanotechnol.*, 2013, **12**, 255–262.
16 N. A. Travlou, K. Singh, E. Rodríguez-Castellón and T. J. Bandosz, *J. Mater. Chem. A*, 2015, **3**, 11417–11429.
17 B. Ghaddab, F. Berger, J. B. Sanchez and C. Mavon, *Procedia Eng.*, 2010, **5**, 115–118.
18 N. Sano, M. Kinugasa and F. Otsuki, *Adv. Powder Technol.*, 2007, **18**, 455–466.
19 J. Meulenbelt, *Medicine (Baltimore).*, 2011, **40**, 94–95.
20 C. P. Hsu, Z. Hejazi, E. Armagan, S. Zhao, M. Schmid, H. Zhang, H. Guo, L. Weidenbacher, R. M. Rossi, M. M. Koebel, L. F. Boesel and C. Toncelli, *Sensors Actuators, B Chem.*, 2017, **488**, 714–722.
21 Y. A. Jaramillo, *Tesis*, 2009, 75.
22 M. Ganiga and J. Cyriac, *Sensors Actuators B. Chem.*, 2016, **225**, 522–528.
23 D. Waller, *Clinical Pharmacology and Poisoning*, London, First., 2016.
24 M. Eising, C. Eduardo, R. Villegas, A. José, G. Zarbin and L. Stolz, *Sensors Actuators B. Chem.*, 2017, **245**, 25–33.
25 K. R. C. Buzea, I.. I. Pacheco Blandino, *Biointerphases*, 2007, **2**, 17–71.
26 E. Roduner, *Chem. Soc. Rev.*, 2006, **35**, 583–592.
27 M. W. C. C. Greenshields, M. A. Mamo, N. J. Coville, I. Chapaval, J. Guilherme, M. V Porsani, A. Bozza and I. A. Hümmelgen, *Sensors Actuators B Chem.*, 2013, **188**, 378–384.

28 M. W. C. C. Greenshields, B. B. Cunha, M. A. Mamo, N. J. Coville and I. A. Hümmelgen, *Int. J. Electroact. Mater.*, 2015, **3**, 10–14.
29 R. Rodrigues and I. A. Hümmelgen, *J. Solid State Electrochem.*, 2016, **20**, 1295–1301.
30 X. Zhou, J. Liu, C. Wang, P. Sun, X. Hu, X. Li and G. Kengo ShimanoeLu, *Sensors Actuators B. Chem.*, 2015, **206**, 577–583.
31 S. S. Gqoba, University of the Witwatersrand, 2018.
32 https://conquerscientific.com/lab-equipment/mass-spectrometers-gcms-systems/.
33 https://www.agilent.com/cs/library/specifications/Public/5989-3290EN.pdf.
34 L. He, Y. Jia, F. Meng, M. Li and J. Liu, *Mater. Sci. Eng. B*, 2009, **163**, 76–81.
35 R. Ghosh, A. Midya, S. Santra, S. K. Ray and P. K. Guha, *Appl. Mater. Interfaces*, 2013, **5**, 7599–7603.
36 B. K. Mutuma, R. Rodrigues, K. Ranganathan, B. Matsoso, D. Wamwangi, I. A. Hümmelgen and N. J. Coville, *J. Mater. Chem. A*, 2017, **5**, 2539–2549.
37 F. Rigoni, G. Drera, S. Pagliara and A. Goldoni, *Carbon N. Y.*, 2014, **80**, 356–363.
38 R. W. Catterall, *Principles of Chemical and Biological Sensors*, Wiley, 1998.
39 J. Fraden, *Handbook of Modern sensors physics, designs, and applications*, Springer, Kong, Hong, 3rd edn., 2003.
40 S. Nagl and O. S. Wolfbeis, , DOI:10.1007/4243.
41 A. J. Bandodkar and J. Wang, *Trends Biotechnol.*, 2014, **32**, 363–371.
42 P. Gründler, *Chemical Sensors An Introduction for Scientists and Engineers*, Springer, Dresden, 2007.
43 J. D. Zook, in *Encyclopedia of Sensors*, eds. E. C. D. and Craig A. Grimes and M. V. Pishko, American Scientific, Dresden, 2006, vol. 9, pp. 329–359.
44 A. Hulanicki, S. Glab and F. Ingman, *Pure&App/. Chern.*, 1991, **63**, 1247–1250.
45 L. Escalona, L. Manganiello and C. V. Martha Lopez – Fonseca, *Rev. Ing. UC*, 2012, **19**, 74–88.
46 V. Montês and M. Química, Universidade do Porto, 2015.
47 E. Bakker and M. Telting-diaz, *Anal. Chem*, 2002, **74**, 2781–2800.
48 B. R. Eggins, *Chemical Sensors and Biosensors*, Wiley, 2004.
49 F.-G. Banica, *Chemical Sensors and Biosensors: Fundamentals and Applications*, JohnWiley & Sons, Ltd., 1st edn., 2012.
50 M. C. Lonergan, E. J. Severin, B. J. Doleman, S. A. Beaber, R. H. Grubbs and N. S. Lewis, *Chem. Mater*, 1996, **8**, 2298–2312.
51 V. Patel, M. W. Jenkins, R. C. Hughes, W. G. Yelton and A. J. Riccol, *Anal. Chem.*, 2000, **72**, 1532–1542.
52 R. Rodrigues, UFPR, 2018.
53 A. V Shevade, M. L. Homer, C. J. Taylor, H. Zhou, A. D. Jewell, K. S. Manatt, A. K. Kisor, S. S. Yen and M. A. Ryan, *Electrochem. Soc.*, 2006, **153**, 209–216.
54 J. T. Robinson, F. K. Perkins, E. S. Snow, Z. Wei and P. E. Sheehan, *Nano Lett.*, 2008, **8**, 3137–3140.
55 D. Wei, Y. Liu, Y. Wang, H. Zhang, L. Huang and G. Yu, *Nano Lett.*, 2009, **9**, 1752–1758.
56 W. Muangrat, E. Gallnom, C. Issro, W. Pfeiler and V. Pierron-bohnes, *Songklanakarin J. Sci. Technol.*, 2012, **34**, 695–699.
57 W. Y. and G. Shi, *J. Mater. Chem. A*, 2013, **1**, 10078–10091.
58 M. Gautam and A. H. Jayatissa, *Mater. Sci. Eng. C*, 2011, **31**, 1405–1411.
59 G. Chen, T. M. Paronyan, A. R. Harutyunyan, G. Chen, T. M. Paronyan and A. R. Harutyunyan, *Appl. Phys. Lett.*, 2012, **101**, 053119.

60 F. Yavari, Z. Chen, A. V Thomas, W. Ren, H. Cheng and N. Koratkar, *Sci. Rep.*, 2011, **166**, 1–5.
61 Y. Zhou, X. Li, Y. Wang, H. Tai and Y. Guo, *Anal. Chem.*, 2018, **91**, 3311–3318.
62 X. Huang, N. Hu, R. Gao, Y. Yu, Y. Wang, A. Zhi Yang Eric Siu-Wai Kong and H. W. and Y. Zhang, *Chem, J Mater*, 2012, **22**, 22488–22495.
63 S. Cui, H. Pu, G. Lu, Z. Wen, E. C. Mattson, C. Hirschmugl, M. Gajdardziska-josifovska, M. Weinert and J. Chen, *Appl. Mater. Interfaces*, 2012, **4**, 4898−4904.
64 R. Lalauze, *Physical Chemistry of Solid-Gas Interfaces: Concepts and Methodology for Gas Sensor Development*, Wiley, 2008.
65 R. F. Taylor, *Handbook of Chemical and Biological Sensors.*, IOP Publishing Ltd., 1996.
66 M. V. Lange U, Roznyatovskaya NV, *Anal Chim Acta*, 2008, **614**, 1–26.
67 A. Kühnle, *Curr. Opin. Colloid Interface Sci.*, 2009, **14**, 157–168.
68 T. M. Letcher and A. L. Myers, in *Chemical Thermodynamics for Industry*, Royal Society Of Chemistry, Cambridge, 2004, pp. 243–253.
69 F. D. Sandoval-ibarra, J. L. López-cervantes and J. Gracia-fadrique, *Educ. Química*, 2015, **26**, 307–313.
70 P. S. Ghosal and A. K. Gupta, *J. Mol. Liq.*, 2017, **225**, 137–146.
71 I. Cruz Cruz, Universidad Autonoma San Luis Potosi, 2011.
72 J. G. Webster, *Measurement, Instrumentation and Sensors*, Taylor & Francis Group, London, 1999.
73 M. Welvaert and Y. Rosseel, *PLoS One*, 2014, **8**, e77089.
74 J. Janata, *Principles of Chemical Sensors*, Springer, Atlanta, 2nd edn., 2009.
75 G. W. and J. T.A., *Sensors, A Comprehensive Survey, Chemical and Biochemical Sensors,Part I*, Weinheim, New York, 2nd edn., 1991.
76 A. Shrivastava and V. Gupta, *Chronicles Young Sci.*, 2011, **2**, 21–25.
77 H. Rahman and M. M. Rahman, *Ann. Bangladesh Agric.*, 2015, **19**, 55–65.
78 J. Mcneill, D. G. Pearson, G. M. Nowell, C. J. Ottley and I. Chinn, *J. Phys. Condens. MATTER*, 2009, **21**, 364207-364207–13.
79 T. Hübert, J. Majewski, U. Banach, M. Detjens and C. Tiebe, in *Proceedings of 7th International Conference on Hydrogen Safety (ICHS 2017)*, Hamburg, 2013, pp. 1–11.
80 R. Zhang and Y. Wang, *Sensors*, 2018, **18**, 2211.
81 G. Wyszecki and W. S. Stiles, *Color Science: Concepts and Methods, Quantitative Data and Formulae*, Wiley, New York, 2nd edn., 1982.
82 E. T. Haugan and P. Dalsjø, *Characterization of the material properties of two FR4 printed circuit board laminates*, 2013.
83 B. K. Mutuma, C. I. Garcia-Martinez, R. C. Dias, B. J. Matsoso, N. J. Coville and I. A. Hümmelgen, *New J. Chem.*, 2019, **43**, 8418–8427.
84 I. B. Usman, C. I. Garcia-Martinez, B. J. Matsoso, D. Wamwangi, I. Cruz-Cruz, J. P. M. Serbena and N. J. Coville, *To be Submitt.*
85 I. B. Usman, B. Matsoso, K. Ranganathan, D. Naidoo, N. J. Coville and D. Wamwangi, *Mater. Chem. Phys.*, 2018, **209**, 280–290.
86 S. Liu, X. Hong, D. Wang, Y. Li, J. Xu, C. Zheng and K. Xie, *Electrochim. Acta*, 2018, **279**, 10–18.
87 S. Li, A. Pasc, V. Fierro and A. Celzard, *J. Mater. Chem. A*, 2016, **4**, 12686–12713.
88 Y. Song, Y. Li and X. Xia, *Electrochem. Commun. 9*, 2007, **9**, 201–205.
89 X. Sun and Y. Li, *J. Colloid Interface Sci. 291*, 2005, **291**, 7–12.
90 Z. Wen, *Electrochem. Commun. 9*, 2007, **9**, 1867–1872.

91 S. Dölle, B. D. Lechner, J. H. Park, S. Schymura, J. P. F. Lagerwall and G. Scalia, *Angew. Chemie - Int. Ed.*, 2012, **51**, 3254–3257.

92 P. Shankar, J. Bosco and B. Rayappan, *Sci. Jet*, 2015, **4**, 126.

93 M. W. C. C. Greenshields, I. A. Hümmelgen, M. A. Mamo, A. Shaikjee, S. D. Mhlanga, W. A. L. Van Otterlo and N. J. Coville, *J. Nanosci. Nanotechnol.*, 2011, **11**, 10211–10218.

94 D. L. Dyre, J. C.; Maass, P.; Roling, B.; Sidebottom, *Reports Prog. Phys.*, 2009, **72**, 046501.

95 T. B. Dyre, J. C.; Schrøder, *Rev. Mod. Phys.*, 2000, **72**, 873.

96 B. Chitara, D. J. Late, S.B. Krupanidhi and C. N. R. Rao, *Solid State Commun.*, 2010, **150**, 2053–2056.

97 G. Gustafsson, I. Lundström, B. Liedberg, C. R. Wu, O. Inganäs and O. Wennerström, *Synth. Met.*, 1989, **31**, 163–179.

98 E. Bekyarova, T. Davis, M. and Burch, M. E. Itkis, B. Zhao, S. Sunshine and R. C. Haddon, *J. Phys. Chem. B*, 2004, **108**, 19717–19720.

99 T. Kimura and E. Al., *Appl. Phys*, 2009, **105**, 014503.

100 K. Singh, N. A. Travlou, S. Bashkova and E. R.-C. T. J. Bandosz, *Carbon N. Y.*, 2014, **80**, 183–192.

101 M. Travlou, Nikolina A. Seredych, R.-C. Enrique and T. J. Bandosz, *J. Mater. Chem. A*, 2015, **3**, 3821–3831.

102 Camille Petit, K. Kante and T. J. Bandosz, *Carbon N. Y.*, 2010, **48**, 654–667.

103 N. Qin, X. Wang and Q. X. and J. Xu, *Sensors Actuators B Chem.*, 2014, **191**, 770–778.

104 S. J. Pearton, F. Ren, Y.-L. Wang, B. H. Chu, K. H. Chen, C. Y. Chang and W. L. J. L. D. P. Norton, *Prog. Mater. Sci.*, 2010, **55**, 1–59.

105 S. J. Pearton, C. Y. Chang, B. H. Chu, C. Lo, F. Ren, W. Chen and J. Guo, *J. Sel. Top. Quantum Electron.*, 2011, **17**, 1092–1101.

106 N. L. Lala and S. Thavasi, Velmurugan Ramakrishna, *Sensors*, 2009, **9**, 86--101.

107 A. Jafari and A. Amini, *Mater. Lett.*, 2019, **236**, 175–178.

108 F. Réti, M. Fleischer, H. Meixner and J. Giber, *Sensors Actuators B Chem.*, 1994, **18**, 138–142.

109 F. Réti, M. F. J. Gerblinger, U. Lampe, E. B. Várhegyi, I. V. Perczel, H. Meixner and J. Giber, *Sensors Actuators B Chem.*, 1995, **26**, 103–107.

110 T. Tsai, S. Chang, W. Weng and S. Liu, *Sensors J.*, 2013, **13**, 4891–4896.

111 D. Zhang and J. T. and B. Xia, *Sensors Actuators B Chem.*, 2014, **197**, 66–72.

112 Y. Yong, H. Cui, Q. Zhou and X. Su, *RSC Adv.*, 2017, **7**, 51027–51035.

# APPENDIX 1–EVALUATION OF DIFERENT ANALYTES

During the development of this work, other analytes were evaluated and selected at the same time, based on both their different properties (Table A1) and the need for evaluating their chemical vapor sensing properties for other projects in the research group of Organic optoelectronic device (GOOD). The discussion about these results was similar to that carried out on this dissertation, as shown elsewhere,[83,84] however it will not be detailed in this document so as not to lengthen it.

Table A1– Properties of the various analytes

| Analyte | Chemical formula | Nature of Solvent | Dielectric constants ($\varepsilon$) | Dipole moment (D) | Vapour pressure (kPa) | Density (g/mL) | Molar mass (g/mol) |
|---|---|---|---|---|---|---|---|
| **Water** | $H_2O$ | Polar protic | 78.50 | 1.85 | 3.16 | 1.00 | 18.02 |
| **Lactic acid** | $C_3H_6O_3$ | Polar protic | 22.00 | 2.66-2.8 | 0.007 | 1,21 | 90.08 |
| **Ammonium Hydroxide** | $NH_4OH$ | Polar protic | 31.60 | 1.46 | 48.00 | 0.91 | 35.05 |
| **Methanol** | $CH_3OH$ | Polar protic | 32.60 | 1.70 | 16.90 | 0.79 | 32.04 |
| **Acetone** | $C_3H_6O$ | Polar aprotic | 17.70 | 2.88 | 30.60 | 0.79 | 58.08 |
| **Toluene** | $C_7H_8$ | Apolar | 2.40 | 0.36 | 3.79 | 0.86 | 92.14 |
| **Chloroform** | $CHCl_3$ | Apolar | 4.80 | 1.12 | 22.62 | 1.49 | 119.38 |

- **Sensors based on annealed HCSs, N-HCSs-10 and N-HCSs-50**

In the Figs. A1-A7 the sensor responses for annealed HCSs and N-HCSs nanostructures are shown. The analysis about the behavior of these sensors when exposed to the several analytes was reported elsewhere.[83]

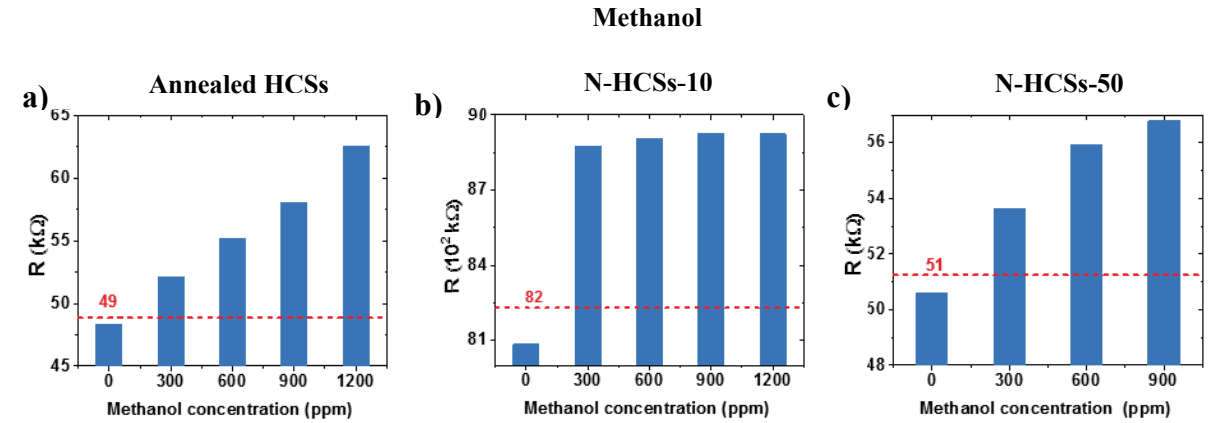


Figure A1 – Data set for sensors when they are exposed to methanol. (a–c) Sensor resistance as a function of analyte concentration, with the red line indicating the estimated *LoD* resistance for the corresponding sensor.

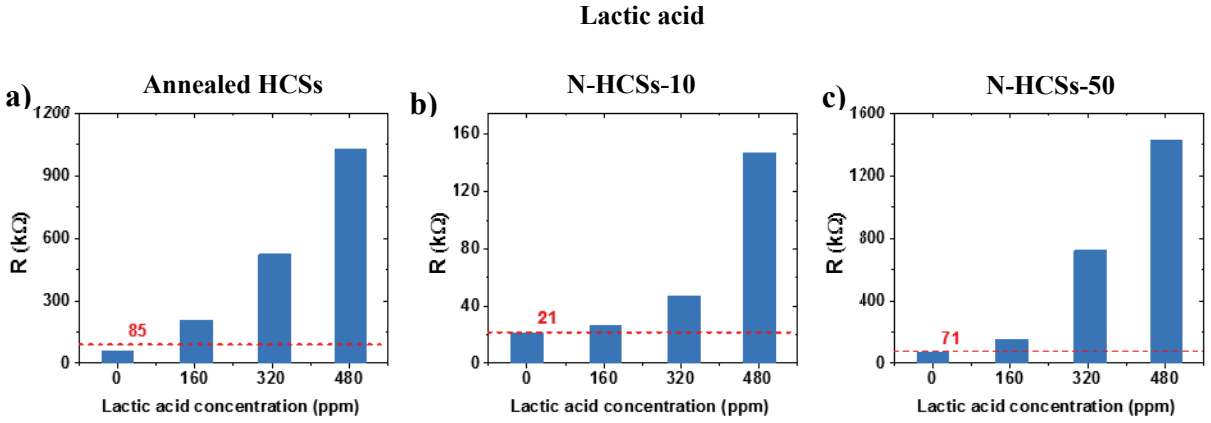


FigureA2 – Data set for sensors when they are exposed to lactic acid. (a–c) Sensor resistance as a function of analyte concentration; the red line indicates the estimated *LoD* resistance for the corresponding sensor.

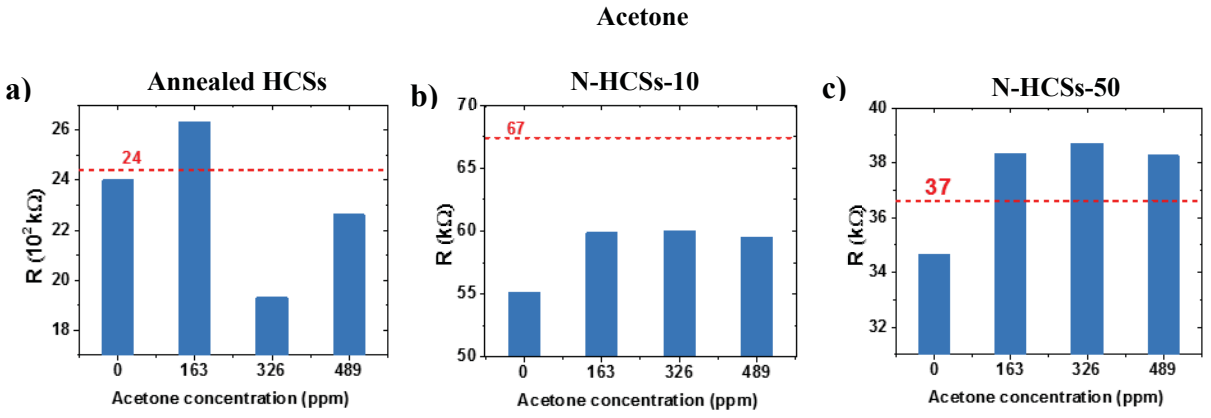


Figure A3 – Data set for sensors when they are exposed to acetone. (a–c) Sensor resistance as a function of analyte concentration; the red line indicates the estimated *LoD* resistance for the corresponding sensor.

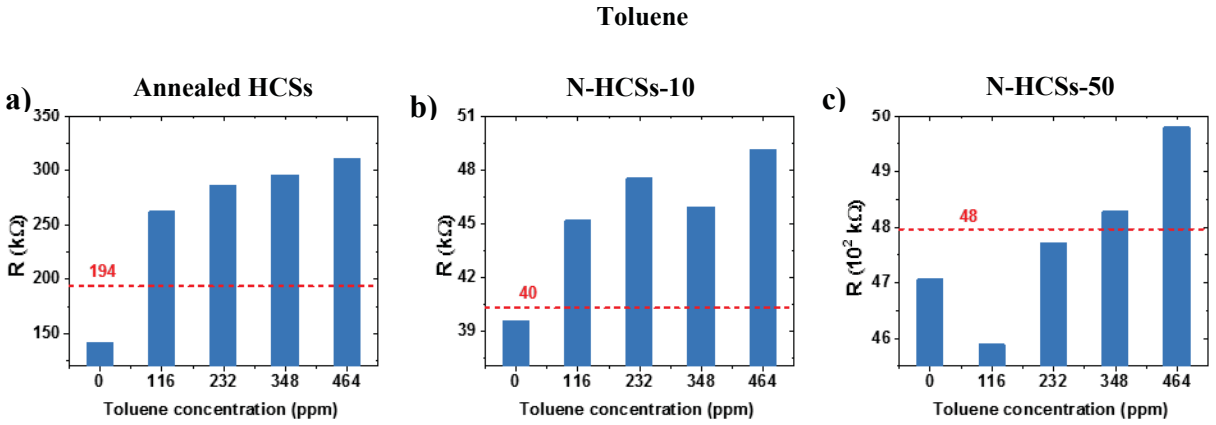


FigureA4 – Data set for sensors when they are exposed to toluene. (a–c) Sensor resistance as a function of analyte concentration; the red line indicates the estimated *LoD* resistance for the corresponding sensor.

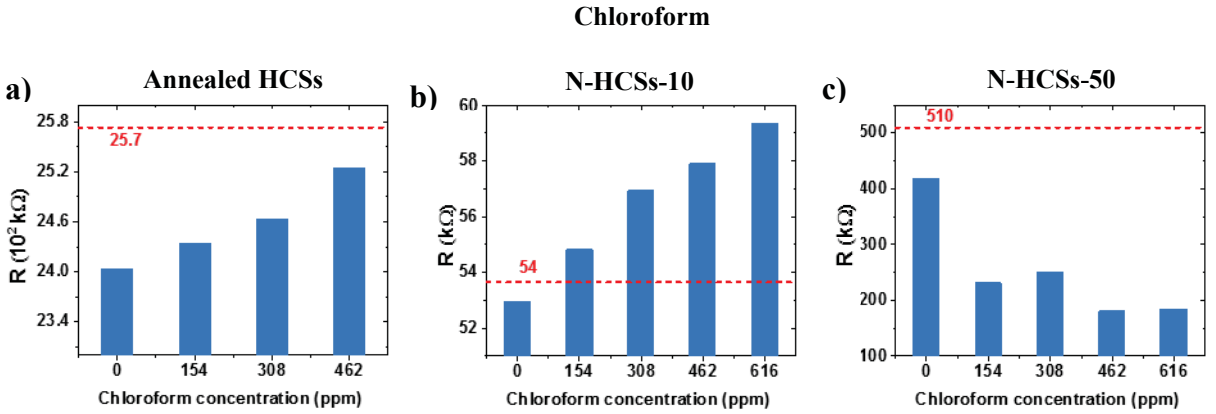


Figure A5 – Data set for sensors when they are exposed to chloroform. (a–c) Sensor resistance as a function of analyte concentration with a red line indicating the estimated *LoD* resistance for the corresponding sensor.

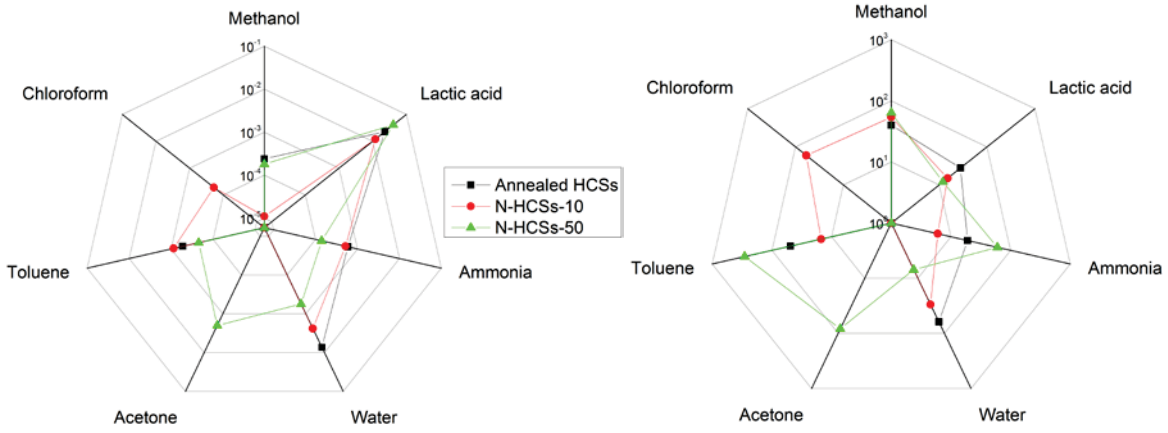


Figure A6 – Logarithmic radar plots for (a) sensitivities ($ppm^{-1}$) and (b) limit of detection (ppm) for HCSs-based sensors at optimized frequencies. Absent values could not be determined due to low signal-to-noise ratio.

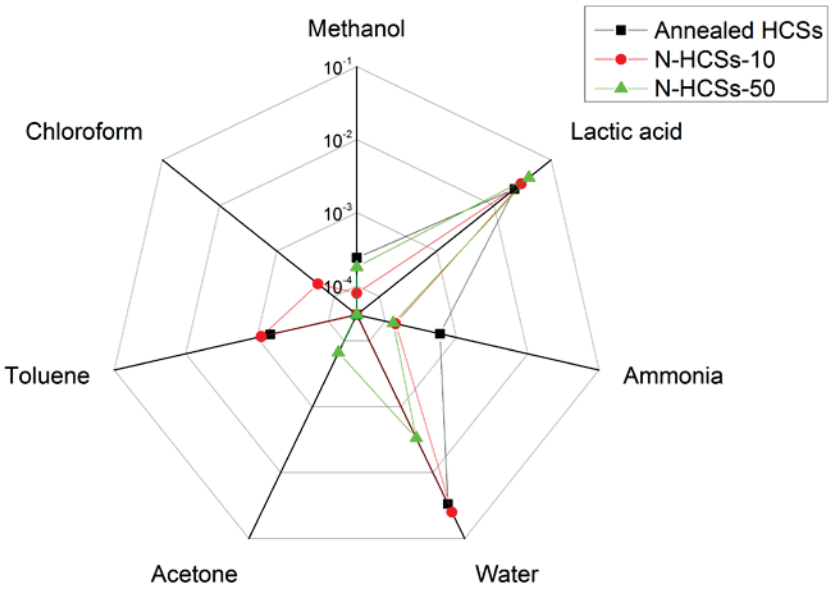


Figure A7 – Sensitivities (in $ppm^{-1}$) in logarithmic radar plot for HCSs-based sensors at 6 kHz.

## ➢ Sensors based on carbon coated GaN (C-GaN)

In the Figs. A8-A13 the sensor responses for both GaN and C-GaN nanoparticles, when exposed to several analytes, are shown.

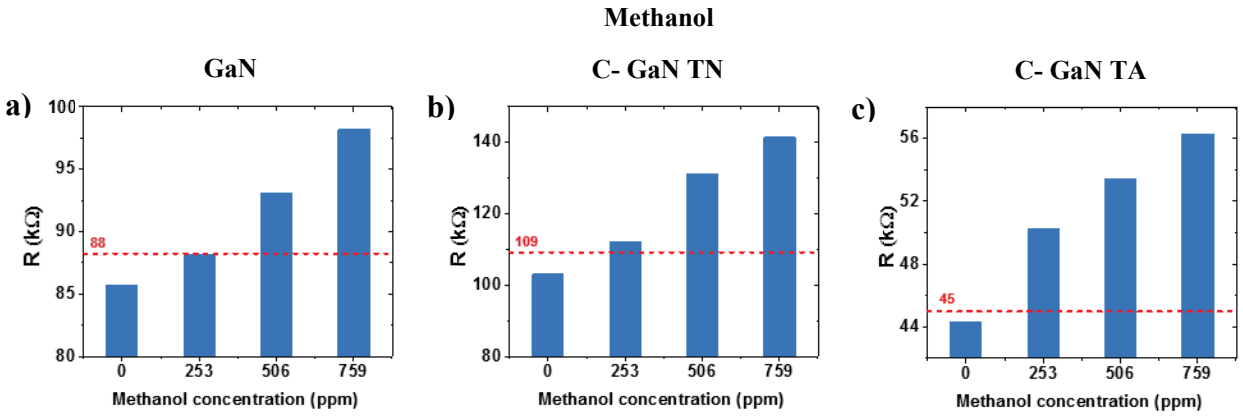


Figure A8 – Data set for sensors when they are exposed to methanol. (a–c) Sensor resistance as a function of analyte concentration; the red line indicates the estimated *LoD* resistance for the corresponding sensor.

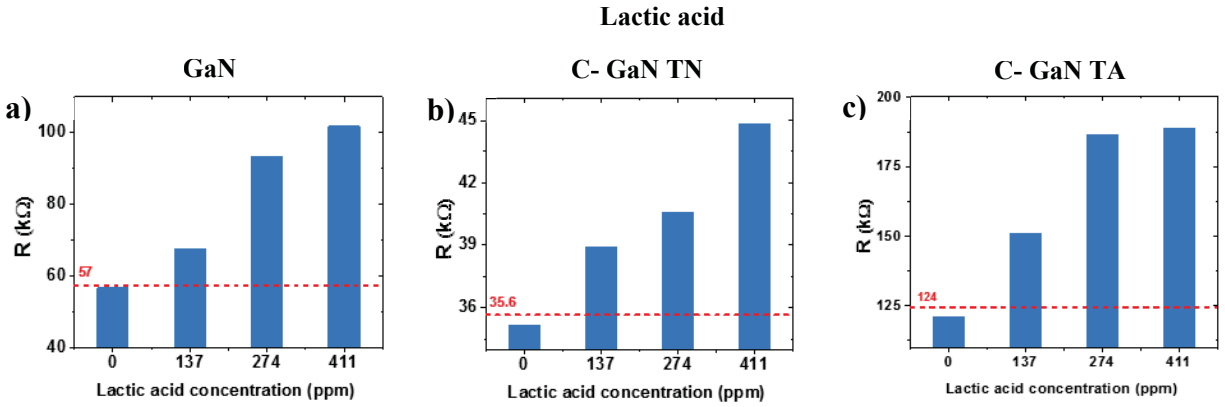


Figure A9 – Data set for sensors when they are exposed to lactic acid. (a–c) Sensor resistance as a function of analyte concentration; the red line indicates the estimated *LoD* resistance for the corresponding sensor.

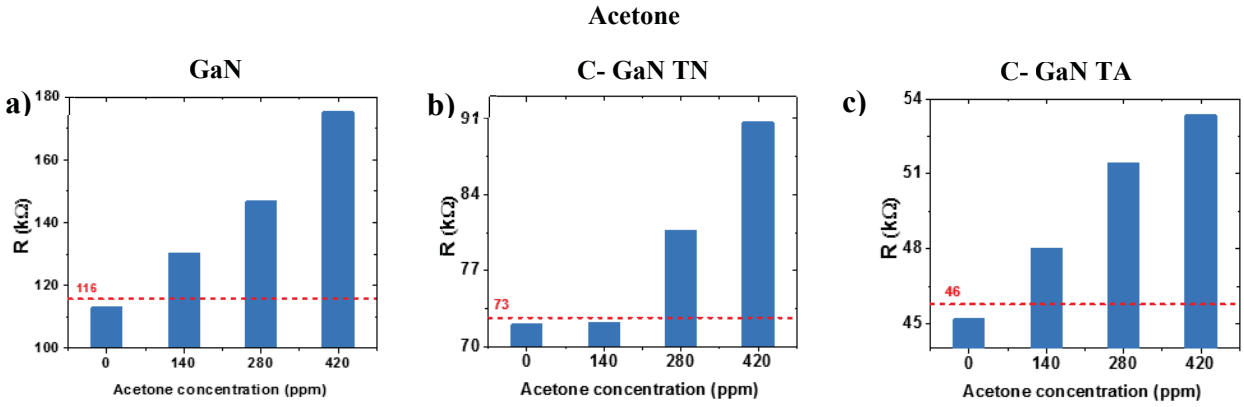


Figure A10 – Data set for sensors when they are exposed to acetone. (a–c) Sensor resistance as a function of analyte concentration with the red line indicating the estimated *LoD* resistance for the corresponding sensor.

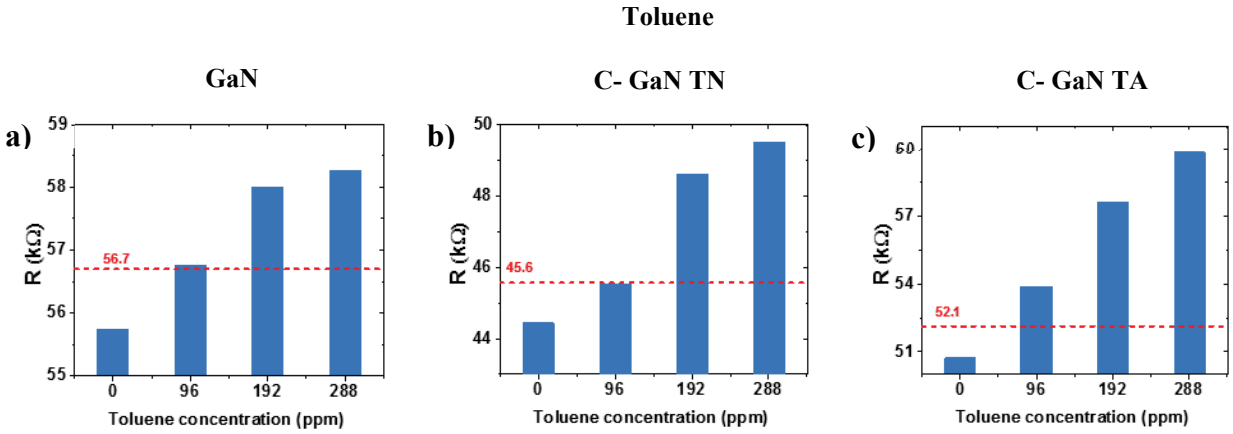


Figure A11 – Data set for sensors when they are exposed to toluene. (a–c) Sensor resistance as a function of analyte concentration; the red line indicates the estimated *LoD* resistance for the corresponding sensor.

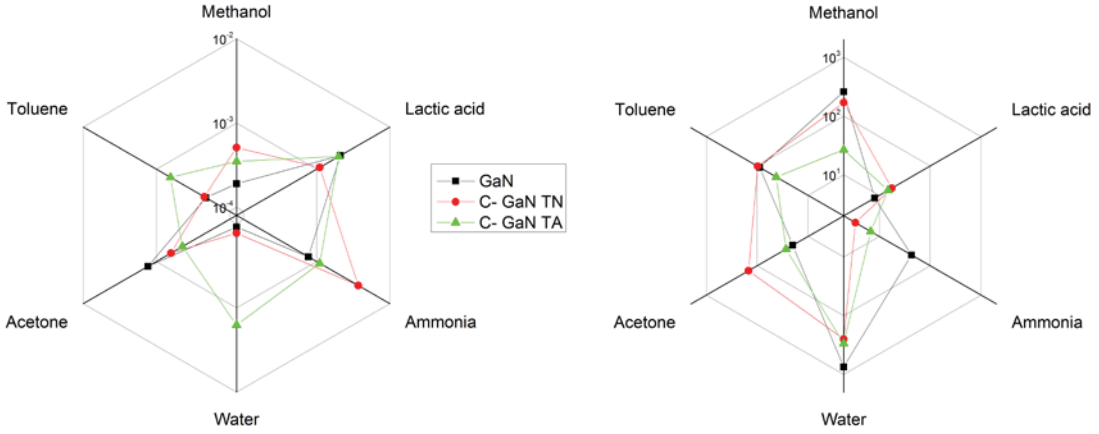


Figure A12 – Logarithmic radar plots for (a) sensitivities ($ppm^{-1}$) and (b) *LoD* (ppm) for GaN-based sensors at optimized frequencies.

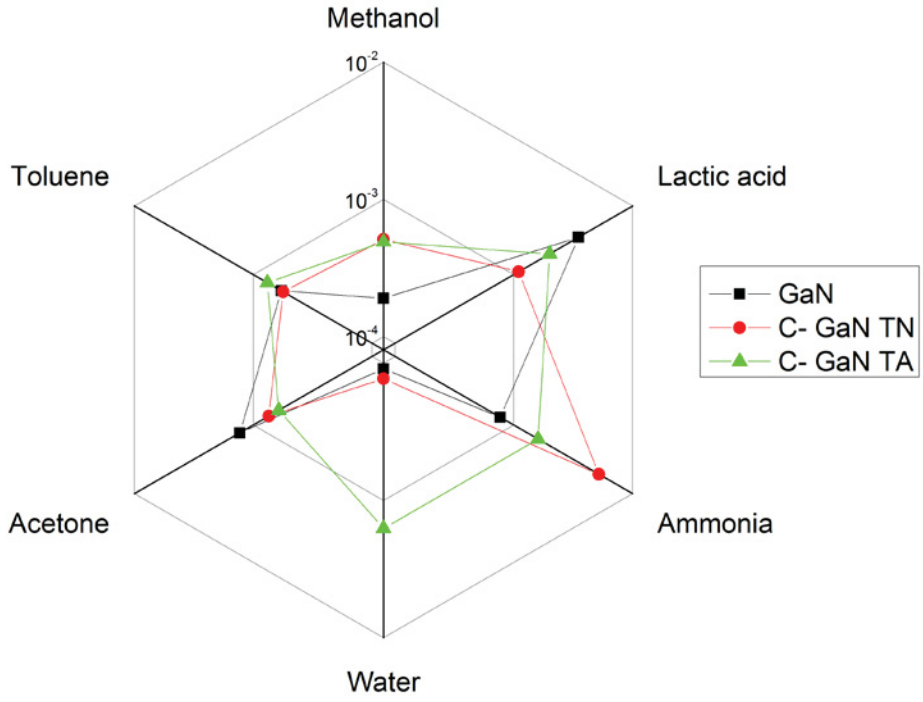


Figure A13 – Sensitivities (in $ppm^{-1}$) in logarithmic radar plot for GaN-based sensors at 3 kHz.

➢ **Sensors based on aligned nitrogen doped multi-walled carbon nanotubes (A-CNTs)**

Sensors based on A-CNTs (x = 0, x = 0.5, x = 1) showed no response to most of the analytes showed (Figs. A14-A17).

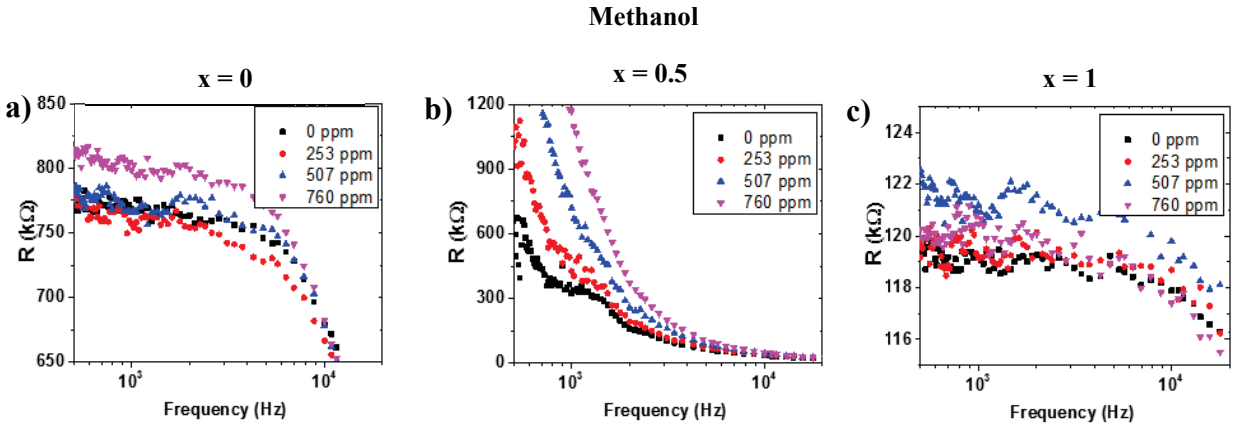


Figure A14 – Data set for sensors when they are exposed to methanol. (a–c) Sensor resistance as a function of the frequency.

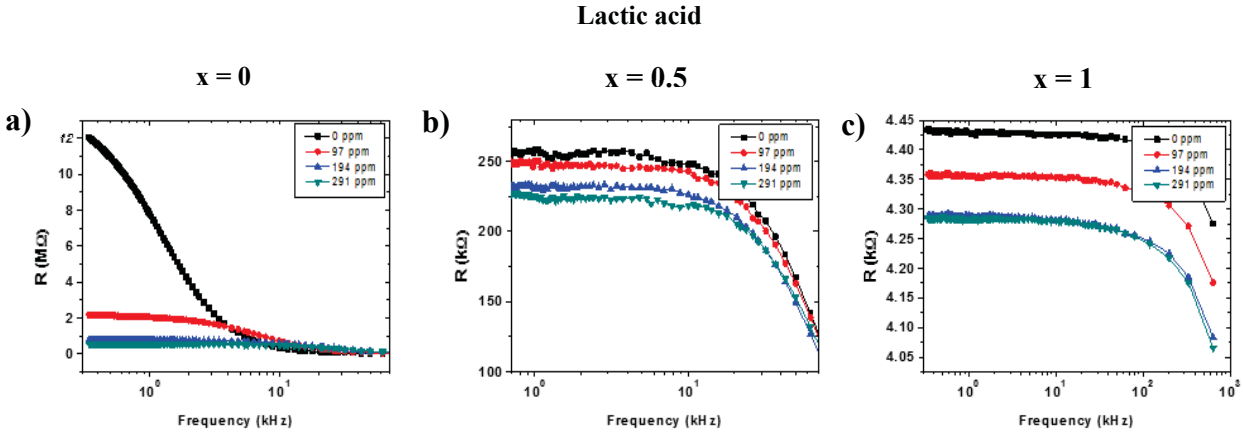


Figure A15 – Data set for sensors when they are exposed to lactic acid. (a–c) Sensor resistance as a function of the frequency.

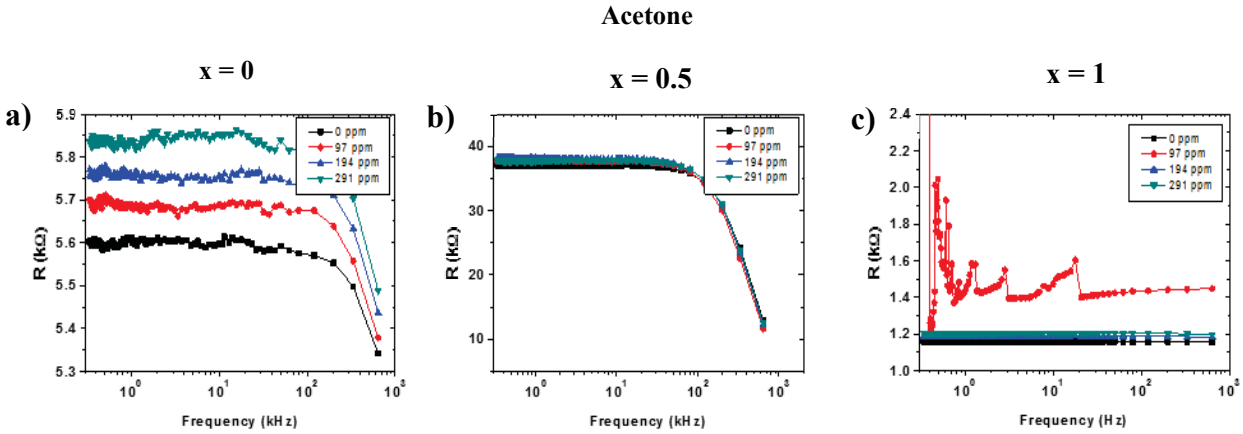


Figure A16 – Data set for sensors when they are exposed to acetone. (a–c) Sensor resistance as a function of the frequency.

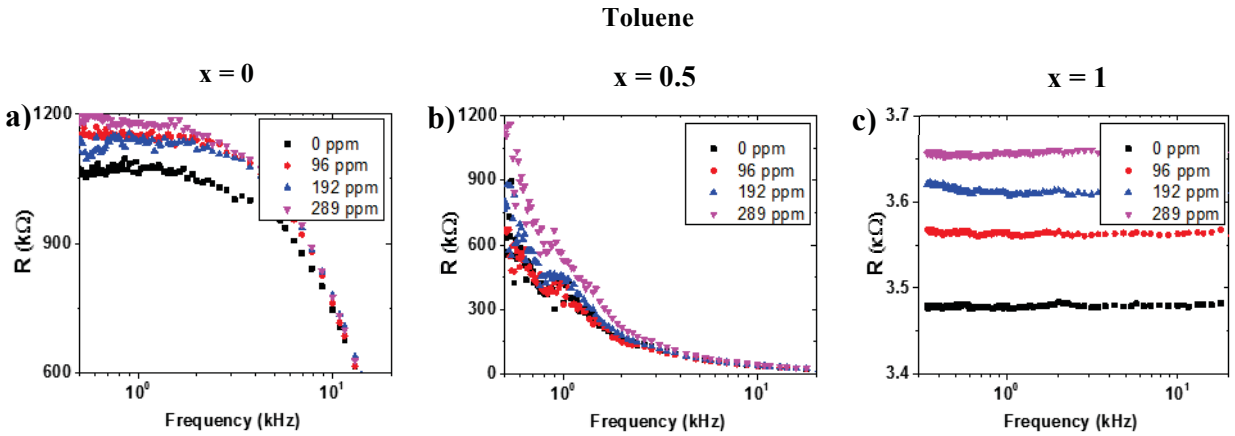


Figure A17 – Data set for sensors when they are exposed to toluene. (a–c) Sensor resistance as a function of the frequency.

# APPENDIX 2 – SCIENTIFIC CONTRIBUTIONS

1. Bridget K. Mutuma, Clara I. Garcia-Martinez, Boitumelo Matsoso, Rodrigo C. Dias, Neil J. Coville and Ivo A. Hümmelgen, *Nitrogen-doped hollow carbon spheres as chemical vapour sensors*, **New Journal of Chemistry**, 2019, DOI: 10.1039/C9NJ00628A. *Back cover of the NJC Journal*.
2. I. B. Usman, C. I. Garcia-Martinez, B. J. Matsoso, D. Wamwangi, I. Cruz-Cruz, J. P. M. Serbena and N. J. Coville, *Sensing properties of carbon coated GaN nanostructures,* **To be Submitted.**

## APPENDIX 3 – PARTICIPATION ON CONGRESS AND/OR COURSES

1. Poster presentation: “Chemical vapor sensors based on nitrogen-doped hollow carbon spheres”, XVIII Brazilian MRS Meeting, in Balneário Camboriú-SC, from 22nd to 26th of September 2019.
2. Summer school on “Micro and Nano Sensors”. Technical University of Denmark. Kongens Lyngby, Denmark. (5 ECTS points) 2019.